Mon. Not. R. Astron. Soc. **384,** 230–250 (2008) doi:10.1111/j.1365-2966.2007.12690.x

Parsec-scale magnetic field structures in *HEAO*-1 BL Lacs

P. Kharb,[1,3]★† D. Gabuzda[2] and P. Shastri[3]
[1]*Department of Physics, Purdue University, West Lafayette, IN 47907, USA*
[2]*University College Cork, Cork, Ireland*
[3]*Indian Institute of Astrophysics (IIA), Bangalore 560034, India*

Accepted 2007 November 7. Received 2007 November 6; in original form 2007 September 17

ABSTRACT

We present very long baseline interferometry polarization images of an X-ray-selected sample of BL Lacertae objects belonging to the first *HEAO-1* and the *ROSAT*–Green Bank (RGB) surveys. These are primarily high-energy-peaked BL Lacs (HBLs) and exhibit core–jet radio morphologies on pc scales. They show moderately polarized jet components, similar to those of low-energy-peaked BL Lacs (LBLs). The fractional polarization in the unresolved cores of the HBLs is, on average, lower than in the LBLs, while the fractional polarizations in the pc-scale jets of HBLs and LBLs are comparable. However, a difference is observed in the orientation of the inferred jet magnetic fields – while LBL jets are well known to preferentially exhibit transverse magnetic fields, the HBL jets tend to display longitudinal magnetic fields. Although a 'spine-sheath' jet velocity structure, along with larger viewing angles for HBLs could produce the observed magnetic field configuration, differences in other properties of LBLs and HBLs, such as their total radio power, cannot be fully reconciled with the different-angle scenario alone. Instead it appears that LBLs and HBLs differ intrinsically, perhaps in the spin rates of their central black holes.

Key words: polarization – BL Lacertae objects: general.

1 INTRODUCTION

BL Lacertae objects are radio-loud active galactic nuclei (AGN) characterized by a predominantly non-thermal, highly polarized continuum, that is variable in total intensity and polarization at all observed wavelengths, and exhibits weak or no optical emission lines (Strittmatter et al. 1972; Stein, Odell & Strittmatter 1976). These extreme phenomena are understood to be a consequence of relativistic beaming in their nuclei (Blandford & Rees 1978; Blandford & Königl 1979). This picture has lead to unification schemes (Urry & Padovani 1995) wherein the low-luminosity Fanaroff–Riley type I radio galaxies (FR I; Fanaroff & Riley 1974) are believed to be the parent population of BL Lac objects, based on similarities in orientation-independent properties such as extended radio emission, emission-line luminosity, host-galaxy type and environment (Browne 1983; Wardle, Moore & Angel 1984a; Prestage & Peacock 1988; Urry & Padovani 1995).

Most BL Lacs discovered before the late 1980s were identified based on radio data (e.g. Ledden & Odell 1985; Burbidge & Hewitt 1987). However, space-based X-ray surveys were highly efficient in discovering new BL Lac objects (e.g. Giommi et al. 1989; Stocke et al. 1989). The observed spectral energy distributions (SEDs) of the X-ray-selected and radio-selected BL Lacs are systematically different. The majority of X-ray-selected BL Lacs show a synchrotron emission peak in the ultraviolet (UV)/soft X-ray regime making them 'high-energy-peaked BL Lacs' or HBLs, while most radio-selected BL Lacs show synchrotron emission peaks in the near-infrared/optical making them 'low-energy-peaked BL Lacs' or LBLs (Giommi & Padovani 1994; Padovani & Giommi 1995). The approximate division between LBLs and HBLs has been defined as $\log(f_x/f_r) \sim -5.5$ (Perlman 1994; Perlman et al. 1996; Wurtz, Stocke & Yee 1996) where f_x and f_r are the 1-keV X-ray and 5-GHz radio flux density, respectively. HBLs are defined as BL Lacs that have $\log(f_x/f_r) \geqslant -5.5$.

LBLs are typically more core-dominated on kpc scales (Perlman & Stocke 1993; Kollgaard, Gabuzda & Feigelson 1996a; Rector et al. 2000; Giroletti et al. 2004b), they display higher average optical polarizations and greater variability (Schwartz et al. 1989; Jannuzi, Smith & Elston 1994), lower starlight fraction (Morris et al. 1991), and have more powerful radio lobes than HBLs (Kollgaard et al. 1992; Laurent-Muehleisen et al. 1993). Based on nuclear trends, it appears that the LBLs are more 'extreme' than HBLs, which in turn has lead to the suggestion that LBLs are oriented at smaller angles to the line of sight than HBLs (Stocke et al. 1985). This scenario is supported by population studies (Padovani & Urry 1990; Urry, Padovani & Stickel 1991a) and has been explained in the framework of an accelerating-jet model, wherein the X-ray photons are emitted in the slower part of the jet and are therefore less beamed

★A major part of this work was completed at IIA, India and JIVE, Holland.
†E-mail: pkharb@physics.purdue.edu

than the radio photons, which are emitted in the faster portion of the jet (Ghisellini & Maraschi 1989; Urry, Padovani & Stickel 1991b). However, the inadequacy of the orientation scenario to explain the systematic differences in the SED peaks of the HBLs and LBLs has given rise to the alternative scenario wherein the X-ray emitting regions of HBLs have higher electron Lorentz factors and/or magnetic field strengths than LBLs (Sambruna, Maraschi & Urry 1996). Georganopoulos & Marscher (1998) have invoked a model that couples jet orientation and electron kinetic luminosity to unify the BL Lac subclasses.

The apparent 'blazar sequence' of increasing synchrotron peak frequency with decreasing source luminosity, as observed in the average SEDs of flat-spectrum radio quasars (FSRQs), LBLs and HBLs (see Sambruna et al. 1996; Fossati et al. 1998; Maraschi & Tavecchio 2001) has been challenged by the discovery of high-energy-peaked FSRQs (Sambruna 1997; Perlman et al. 1998; Padovani et al. 2002) and high-luminosity HBLs (Giommi et al. 2005). In addition, the gap between LBLs and HBLs has now been filled with the discovery of intermediate-peak BL Lacs (IBLs) which have SED peaks in the optical/UV wavebands and exhibit intermediate properties between LBLs and HBLs (Kock et al. 1996; Nass et al. 1996; Perlman et al. 1998; Laurent-Muehleisen et al. 1999; Stevens & Gear 1999). Thus the question of HBLs and LBLs being two distinct AGN classes, as opposed to being the extreme ends of a continuous distribution of BL Lac properties, is an open one.

Owing to their relatively greater radio flux densities, LBLs have been the subject of extensive very long baseline interferometry (VLBI) observations (e.g. Gabuzda, Pushkarev & Cawthorne 2000; Kellermann et al. 2004; Lister & Homan 2005). These studies have found them to be typically compact, with a core and a relatively small number of fairly discrete jet components. Measured superluminal speeds are typically modest, in the range of $2c$–$4c$ (Gabuzda et al. 1994, 2000; Kellermann et al. 2004). VLBI polarization (VLBP) observations have shown a number of systematic differences between LBLs and FSRQs, initially detected in images obtained at 5–8 GHz (Gabuzda et al. 1992; Cawthorne et al. 1993; Gabuzda et al. 2000) but generally being retained in the higher frequency 15-GHz images (Lister & Homan 2005) – LBLs have appreciably polarized cores (core fractional polarization, $m_c \sim 2$–5 per cent) with predominantly transverse magnetic (B) fields in their jets, while quasars have weakly polarized cores ($m_c < 2$ per cent) and predominantly longitudinal B fields in their pc-scale jets.

HBL polarization properties have, on the other hand, not been explored as much with VLBI experiments due to their relatively lower radio flux densities. 5-GHz total intensity VLBI images of a sample of HBLs belonging to the *Einstein* 'Slew' Survey were presented by Rector, Gabuzda & Stocke (2003a). They found that HBLs displayed core–jet morphologies similar to the LBLs. However, there was a weak evidence that the HBL jets exhibited smaller misalignments between parsec and kiloparsec scales than LBL jets (see also Giroletti et al. 2004b). This was interpreted as being either due to intrinsically straighter jets in HBLs or their jets being oriented further from the line of sight than LBLs jets. Note however that 8.4-GHz VLA observations of a sample of EMSS and High Energy Astronomy Observatory (*HEAO-1*) BL Lacs failed to show a systematic trend of smaller misalignments in HBL jets (E. Perlman, private communication).

In this paper, we present VLBP observations of a sample of 18 BL Lacs belonging to the *HEAO-1* hard X-ray and the *ROSAT*–Green Bank (RGB) surveys. 13 of these BL lacs have been classified as HBLs. Early VLBP results for four of these *HEAO-1* BL Lacs were presented by Kollgaard et al. (1996a). Sections 2 and 3 describe the BL Lac sample and the observations. We present our results in Sections 4–6. A discussion follows in Section 7, and the conclusions in Section 8. We assume throughout a cosmology where $H_0 = 71$ km s^{-1} Mpc^{-1}, $\Omega_M = 0.24$ and $\Omega_\Lambda = 0.76$.

2 THE SAMPLE

The *HEAO-1* Large Area Sky Survey (LASS) detected 842 hard X-ray (0.8–20 keV) sources over the entire sky (Wood et al. 1984). To date, 29 BL Lacertae objects have been identified in the LASS catalogue (Laurent-Muehleisen et al. 1993), one of which (2201+044) is now known to be a Seyfert 1 galaxy (Veron-Cetty & Veron 1993). Note that 2201+044 is part of our sample. The RGB sample of BL Lacs was generated from a cross-correlation of the *ROSAT* All-Sky Survey (RASS) and a reanalysis of the 1987 Green Bank 6-cm radio survey (Gregory et al. 1996; Laurent-Muehleisen et al. 1997). VLA observations of the *HEAO-1* BL Lac sample have been presented by Laurent-Muehleisen et al. (1993) and Kollgaard et al. (1996a). Here we present VLBP results for nine *HEAO-1* BL Lacs, along with eight BL Lacs belonging to the RGB sample. In all, there are 13 HBLs, four LBLs and one Seyfert 1 galaxy. Of the four LBLs, 1147+245 also belongs to the 1-Jy sample.

The BL Lac sample is presented in Table 1, which has the following columns: columns 1 and 2: IAU and other names; column 3: BL Lac classification based on the SED peak frequency and/or the $\log(f_x/f_r)$ criterion (see cf. Section 1); column 4: sample membership, with H denoting sources belonging to the *HEAO-1* sample, R to the RGB sample and J to the 1-Jy sample; column 5: membership of other 'heritage' X-ray samples: RX = RASS, 1E, 2E and ES = *Einstein* Survey, second Image Proportional Counter *Einstein* X-ray Survey and *Einstein* 'Slew' Survey, respectively; column 6: redshift; column 7: projected linear scale corresponding to an angular scale of 1 mas; columns 8–10: the epochs for which results are presented here; columns 11 and 12: the references for the redshifts and BL Lac classification, respectively.

3 OBSERVATIONS AND DATA REDUCTION

The polarization observations were made at 5 GHz with (i) a global VLBI array on 1993 February 23 (1993.15) and (ii) on 1995 July 13 (1995.53) and 1998 June 28 (1998.49) with the 10-element Very Large Baseline Array (VLBA[1]; see Table 2). In all cases, each source was observed for a total of roughly 1.3–2.8 h, in 12–26 scans distributed throughout the time the source was observable with all or nearly all of the antennas in the VLB arrays. Two intermediate frequencies (IF, or equivalently, baseband converters) were recorded in each polarization, with 8 MHz per IF, and a total aggregate bit rate of 128 Mbits s^{-1}. The data were correlated by the VLBA correlator in Soccoro. The preliminary calibration, fringe fitting, polarization calibration and imaging were done using the Astronomical Image Processing System (AIPS) following standard methods.

3.1 Global VLBI

The global VLBI array used for the 1993 February 23 observations included the Effelsberg (EB), Green Bank (GB), and Medicina (MC) telescopes, the phased Very Large Array (Y27), and the Hancock

[1] The VLBA is operated by the National Radio Astronomy Observatory, which is a facility of the National Science Foundation operated under cooperative agreement by Associated Universities, Inc.

Table 1. Properties of the sample BL Lacs.

IAU name	Other name	Class	Sample	X-ray sample	z	Scale (pc mas^{-1})	Epochs 1993.15	Epochs 1995.53	Epochs 1998.49	z reference	Class reference
0414+009		HBL	H	RX, 2E	0.287	4.285	X	X		1	15
0652+426	4C 42.22	HBL	R	RX	0.0590	1.127			X	2	16
0706+592		HBL	H	RX	0.1250	2.215	X	X		2	16
0749+540	4C 54.15	LBL	R	RX	>0.20	3.268			X	3	16
0829+046	OJ049	LBL	R	RX	0.1736	2.918	X	X	X	4	16
0925+504		LBL*	R	RX	0.3703	5.090			X	5	17
1011+496		HBL	H	ES	0.212	3.268			X	6	16
1101+384	Mrk 421	HBL	H	RX, ES	0.0300	0.593		X	X	7	15
1133+704	Mrk 180	HBL	H	RX, ES	0.0452	0.877			X	8	15
1147+245		LBL	J	–	>0.20	3.268		X		9	16
1215+303	ON 325	HBL	H	ES	0.1300	2.291	X		X	10	15
1227+255		HBL*	R	RX	0.1350	2.366			X	11	17
1235+632		HBL*	H	RX, 1E	0.2969	4.389	X			10	18
1553+113		HBL*	R	RX, ES	0.3600	4.998			X	12	15
1727+502	I Zw 187	HBL	H	RX, ES	0.0554	1.062		X	X	13	16
1741+196		HBL	R	RX, ES	0.0840	1.559			X	14	15
1743+398		HBL	R	RX	0.2670	4.068			X	2	16
2201+044	4C 04.77	Seyfert 1	H	RX	0.0270	0.535			X	1	19

Notes: *BL Lacs which have been alternately classified as IBLs by Nieppola et al. (2006). Last two columns list references for redshift and BL Lac classification, respectively. (1) Falomo, Scarpa & Bersanelli (1994), (2) Laurent-Muehleisen et al. (1998), (3) Stickel & Kühr (1993), (4) Falomo (1991), (5) Henstock et al. (1997), (6) Albert et. al. (2007), (7) Ulrich et al. (1975), (8) Ulrich (1978), (9) Stickel, Fried & Kühr (1993), (10) Bade et al. (1998), (11) Nass et al. (1996), (12) Hewitt & Burbidge (1987), (13) Oke (1978), (14) Heidt et al. (1999), (15) Donato, Sambruna & Gliozzi (2005), (16) Nieppola et al. (2006), (17) Laurent-Muehleisen et al. (1999), (18) Wurtz et al. (1996), (19) Veron-Cetty & Veron (1993).

(HN), North Liberty (NL), Brewster (BR) and Owens Valley (OV) VLBA antennas. Effelsberg was used as the reference antenna at all stages of the calibration. The unpolarized source OQ 208 was used as the instrumental polarization (*D*-term) calibrator in the AIPS task LPCAL. The absolute electric vector polarization angle (EVPA or χ) calibration was performed by comparing the total VLBI scale and (simultaneously measured) VLA core polarizations for the compact polarized source OJ 287.

3.2 VLBA

The 1995 July 13 and 1998 June 28 observations were obtained using the ten telescopes of the American VLBA. Los Alamos was used as the reference antenna at all stages of the calibration. The unpolarized source 3C84 and the nearly unresolved polarized source 0749+540 were used for the *D*-term calibration for the 1995 July and 1998 June observations, respectively. Short 2–3 min VLA snapshots of 10 *HEAO-1* HBLs, including five of the four HBLs for which 1995.53 images are presented here, were made at 4.9, 8.4 and 15.0 GHz on 1995 July 18, only a few days after the 1995 July VLBA observations. We used the results of these 4.9-GHz observations for OJ287 for the EVPA calibration of the VLBA data, assuming that the polarization position angle (PA) of OJ287 did not vary between the VLA and VLBI observations.

Unfortunately, we did not have integrated polarization measurements of any compact polarized sources observed during our 1998 June VLBA run nearby in time to those VLBA observations. Instead, we applied the EVPA calibration determined for VLBA observations in 1998 March and April, based on integrated polarization measurements within a few days of those experiments and using the same reference antenna (Los Alamos). The EVPA calibration corresponds to the phase difference between the right- and left-hand circularly polarized signals at the reference antenna, and has been shown to be constant to within a few degrees over as long as several years, if no adjustments are made to the receiver affecting this instrumental parameter (Reynolds, Cawthorne & Gabuzda 2001). Our observations were only a few months after those of Charlot et al. (2006); moreover, the EVPA calibration for 5-GHz VLBI observations obtained in 2000 June, based on simultaneous VLA polarization measurements and also reduced using Los Alamos as the reference antenna, indicates that this calibration had remained the same to within a few degrees (Gabuzda, O'Sullivan & Gurvits, private communication), thus justifying the application of the 5-GHz EVPA calibration for the 1998 March–April VLBA observations to our 5-GHz data.

4 RESULTS

The VLBP observations of the 17 sample BL Lacs (and one Seyfert 1 galaxy) reveal core–jet morphologies in all but two sources, viz. 0706+592 and 0749+540. Polarization is detected in the cores and/or jets of all but three sources, viz. 0414+009, 0706+592 and 1235+632. Total intensity images with polarization electric vectors superimposed are presented in Figs 1–14. The Gaussian restoring beam for each object is shown in the lower left-hand corner of the image. The rms noise in the total intensity maps is typically $\sim$100 μJy beam^{-1}.

The polarization electric vectors have not been corrected for Faraday rotation, occurring either in our Galaxy (i.e. an overall rotation of the EVPAs applied to all regions in the source) or in the immediate vicinity of the BL Lac object (likely affecting only certain regions in the source). Multifrequency VLBP observations have demonstrated that the contribution from regions of thermal magnetized plasma in the immediate vicinity of the BL Lac object may be substantial in the core region, but is likely to be relatively small in the jet at appreciable distances from the core (e.g. Zavala & Taylor 2003, 2004). Typical Galactic (i.e. foreground) rotation measures are no more than a few dozen rad m^{-2}, corresponding to rotations at 5 GHz of about 10° or less (e.g. Pushkarev 2001). Thus, we expect that the jet

Table 2. Details of the VLBP observing programme.

Observing date	Frequency (MHz)	Antennas	*D*-term calibrator	EVPA calibrator
1993 February 23	4979.99	MC, EB, WB, GB, Y27 HN, NL, BR, OV	OQ 208	0235+164, OJ 287
1995 July 13	4987.49	VLBA	3C 84	OJ 287
1998 June 28	4991.46	VLBA	0749+540	Other

EVPAs should not be far from their intrinsic values, while the core EVPAs may in principle be subject to appreciable Faraday rotation.

Models for all the sources were derived by fitting the complex, fully calibrated total intensity (*I*, the *RR* and *LL* correlations) and linear polarization (*P*, the *RL* and *LR* correlations) visibilities that result from the mapping process with a small number of circular Gaussian components, as described by Roberts, Gabuzda & Wardle (1987) and Gabuzda, Wardle & Roberts (1989). We checked for consistency between the model fits, the distribution of CLEAN components, and the visual appearance of the images. The *I* and *P* visibilities were fitted separately, in order to allow for small differences in the positions and sizes of corresponding *I* and *P* components, either intrinsic to the source structure or associated with residual calibration errors. The model-fitting results are presented in Table 3, where the columns list the fitted parameters for various epochs (in italics). Column 1 presents the source name, while the remaining columns present for each component; column 2 an identifying label, with C denoting the core; columns 3 and 4 the total (I) and polarized (p) intensities; columns 5 and 6 the polarization PA (χ) and fractional polarization (m); columns 7 and 8 the separation from the core (r) and its uncertainty (Δr); columns 9 and 10 the structural PA (θ) and its uncertainty ($\Delta\theta$); column 11 the size [full width at half-maximum (FWHM)].

Comments on the individual sources follow in Section 5. When interpreting the observed polarization images, we assume that the jet emission is optically thin; in contrast, the observed 'core' emission may be predominantly optically thick or optically thin, depending on the relative contributions of the optically thick 'intrinsic' core and regions of the optically thin innermost jet that are blended with this feature due to our finite spatial resolution.

5 NOTES ON INDIVIDUAL BL LACS

5.1 0414+009

This BL Lac object is hosted by a luminous elliptical that is the dominant member of a galaxy cluster (Falomo & Tanzi 1991). The 5-GHz VLA image of Reid, Kronberg & Perley (1999) shows a jet-like feature at PA $\sim 40^\circ$. Both of our VLBI images (Fig. 1) show a jet in PA $\sim 75^\circ$, with no detected polarization.

5.2 0652+426

The 1.4-GHz VLA image of this source shows a two-sided jet source embedded in a bright halo, with the brighter jet at PA $= 40^\circ$ (Rector et al. 2003a). Our VLBI image (Fig. 2) shows a well-collimated jet extending from the core in PA $\sim 40^\circ$. Polarization is detected in the inner jet, with the inferred *B* field showing no obvious relation to the jet direction.

5.3 0706+592

The 1.4-GHz VLA image of Giroletti et al. (2004b) shows the radio core to be located on the north-west edge of a roughly spherical cocoon. They suggest that this object could be a wide-angle or narrow-angle tailed object, viewed at a small angle. Their 5-GHz VLBA image shows a weak jet to the south-west. Our two VLBI images (Fig. 3) are dominated by a compact core, with weak extensions to the west (in 1993) and south-west (in 1995); given the image of Giroletti et al. (2004b), the former is probably an artefact. We did not detect polarization at either of our epochs.

5.4 0749+540

This source was classified as a BL Lac object by Kühr & Schmidt (1990) based on its featureless optical spectrum and high optical polarization. A lower limit of $z > 0.2$ for its redshift was derived by Stickel & Kühr (1993) based on the absence of any extended structure of a host galaxy in a direct image taken with the 3.5-m Calar Alto Telescope. The 5-GHz VLBI image of Taylor et al. (1994) shows a jet emerging from the core in PA $\sim 0^\circ$. Our VLBI image (Fig. 4) reveals a dominant core, with an extension to the north, in roughly the direction of the previously detected VLBI jet. The core shows an unusually high fractional polarization of $\sim$9 per cent, while no polarization was detected in the jet.

5.5 0829+046

0829+046 or OJ 049 is a γ-ray loud blazar (Dondi & Ghisellini 1995) which shows rapid and large optical variability (Liller & Liller 1975). The 1.4-GHz VLA images of Antonucci & Ulvestad (1985) and Giroletti et al. (2004b) show a two-sided structure with an extended and curved region of emission to the south-east. Previous VLBI images show a VLBI jet extending to the north-east (Jorstad et al. 2001), clearly misaligned with the kpc-scale radio structure. Our VLBI images (Fig. 5) reveal the rich polarization structure of the VLBI jet, whose inferred *B* field geometry has remained roughly constant over about five years. The predominant jet *B* field is longitudinal to the jet. The polarization PA for the knot K4 changes dramatically over the roughly five years covered by our observations, and seems to swing to remain perpendicular to the VLBI jet as this component propagates from the core (making the dominant *B* field longitudinal essentially throughout the jet). Both K3 and K4 show appreciable increases in the degree of polarization accompanied by decreases in total intensity, suggesting this is associated with the expansion of these components as they evolve.

5.6 0925+504

The 1.4-GHz VLA image of Giroletti et al. (2004b) shows a faint jet-like extension to the south-east, while the 8.4-GHz VLA map of

Table 3. *HEAO-1* BL Lac VLBI models.

Source	Component	I (mJy)	p (mJy)	χ (°)	m (per cent)	r (mas)	Δr (mas)	θ (°)	$\Delta\theta$ (°)	FWHM (mas)
0414+009					*1993.15*					
	C	26.9	–	–	–	–	–	–	–	0.02
	K1	8.3	–	–	–	1.43	0.06	72	5	0.96
					1995.53					
	C	38.5	–	–	–	–	–	–	–	0.22
	K1	7.7	–	–	–	1.74	0.23	74	8	2.02
0652+426					*1998.49*					
	C	132.7	–	–	–	–	–	–	–	0.09
	K5	18.7	0.71	−3.2	3.79	1.55	0.03	39	1	0.18
	K4	4.7	–	–	–	3.08	0.12	28	2	0.07
	K3	4.4	–	–	–	6.09	0.30	30	2	1.45
	K2	2.5	–	–	–	5.99	0.20	35	2	0.29
	K1	2.9	–	–	–	11.69	1.84	28	6	4.27
0706+592					*1993.15*					
	C	24.9	–	–	–	–	–	–	–	0.23
					1995.53					
	C	27.7	–	–	–	–	–	–	–	0.19
	K1	1.9	–	–	–	4.05	0.50	-157	7	1.00
0749+540					*1998.49*					
	C	1530.1	148.5	62.7	9.7	–	–	–	–	0.14
	K3	93.2	–	–	–	0.75	0.03	-124	3	0.10
	K2	82.6	–	–	–	0.85	0.03	22	4	0.29
	K1	7.8	–	–	–	4.31	0.26	5	6	2.12
0829+046					*1993.15*					
	C	470.7	15.2	24.9	3.2	–	–	–	–	0.39
	K4	80.8	3.2	4.9	4.0	1.00	0.03	55	2	0.39
	K3	189.6	11.1	–20.8	5.8	2.62	0.01	59	0	1.22
	K2	32.9	15.6	–65.9	47.4	4.08	0.06	50	1	1.65
	K1	20.6	–	–	–	5.21	0.10	51	1	2.74
					1995.53					
	C	674.9	20.1	55.1	2.9	–	–	–	–	0.45
	K5	161.2	9.9	6.9	6.1	1.06	0.01	58	1	0.79
	K4	150.2	8.9	–21.5	5.9	2.58	0.01	66	0	0.44
	K3	48.9	9.8	–40.1	20.0	3.97	0.02	57	0	0.31
	K2	18.2	5.6	–39.5	30.8	5.28	0.07	60	1	0.37
	K1	14.3	1.6	1.2	11.1	7.12	0.08	59	1	1.10
					1998.49					
	C	414.0	18.2	36.2	4.4	–	–	–	–	0.22
	K6	98.3	10.7	–4.7	10.9	1.02	0.02	57	1	0.48
	K5	160.7	7.9	–47.5	4.9	2.52	0.01	67	0	1.03
	K4	24.1	5.9	–70.7	24.5	3.90	0.04	61	1	0.48
	K3	15.2	–	–	–	5.41	0.04	62	1	0.41
	K2	17.7	7.7	–42.6	43.5	7.37	0.13	58	1	2.35
	K1	9.9	–	–	–	9.88	0.19	58	2	1.68
0925+504					*1998.49*					
	C	477.1	67.8	58.7	14.2	–	–	–	–	0.57
	K2	19.1	–	–	–	6.47	0.18	128	1	3.32
	K1	9.8	–	–	–	9.41	2.07	132	11	4.53
1011+496					*1998.49*					
	C	89.3	4.2	–12.2	4.7	–	–	–	–	0.36
	K4	25.9	0.9	–10.3	3.5	1.00	0.01	−110	1	0.27
	K3	9.3	–	–	–	2.12	0.03	−96	1	0.23
	K2	2.1	–	–	–	3.27	0.13	−87	5	0.06
	K1	8.2	0.5	41.9	6.1	6.62	0.09	−102	1	1.86

Table 3 – *continued*

Source	Component	I (mJy)	p (mJy)	χ (°)	m (per cent)	r (mas)	Δr (mas)	θ (°)	$\Delta\theta$ (°)	FWHM (mas)
1101+384					*1995.53*					
	C	318.4	4.8	–87.8	1.5	–	–	–	–	0.17
	K8	35.2	2.7	21.8	7.7	1.24	0.02	−33	1	0.17
	K7	12.1	–	–	–	2.81	0.11	−36	2	1.43
	K6	9.2	2.5	–43.2	27.2	5.37	0.11	−37	1	1.49
	K5	8.2	–	–	–	9.95	0.76	−32	4	4.65
	K4	6.9	–	–	–	15.95	0.78	−34	3	4.43
	K3	6.7	–	–	–	19.19	0.55	−47	2	3.66
	K2	1.6	0.7	–52.5	43.8	20.52	0.63	−62	2	1.55
	K1	26.1	–	–	–	32.13	1.08	−62	2	14.9
					1998.49					
	C	348.3	4.2	–54.3	1.2	–	–	–	–	0.19
	K8	31.8	4.9	–2.6	15.4	1.35	0.03	−40	1	0.43
	K7	5.1	–	–	–	2.96	0.15	−43	3	0.76
	K6	18.3	1.8	–71.0	9.8	5.44	0.14	−41	1	2.41
	K5	18.9	–	–	–	11.96	1.41	−37	5	9.48
	K3	4.1	1.1	–88.0	26.8	19.63	0.61	−52	2	3.35
1133+704					*1998.49*					
	C	97.5	–	–	–	–	–	–	–	0.21
	K6	9.8	2.8	3.9	28.6	1.01	0.10	103	4	1.13
	K5	7.6	1.1	–39.6	14.5	2.99	0.13	106	1	0.04
	K4	2.1	–	–	–	4.72	0.51	92	3	0.66
	K3	4.3	–	–	–	10.54	1.54	78	7	6.11
	K2	1.6	–	–	–	16.89	1.24	77	4	2.68
	K1	0.4	–	–	–	24.77	1.12	68	2	0.03
1147+245					*1995.53*					
	C	432.1	18.6	10.9	4.3	–	–	–	–	0.34
	K6	120.9	–	–	–	0.88	0.01	−103	1	0.66
	K5	55.1	2.9	–84.1	5.3	2.65	0.02	−96	1	1.61
	K4	21.1	2.2	–60.0	10.4	8.35	0.32	−90	1	4.20
	K3	7.0	4.1	–59.4	58.6	8.50	0.11	−88	1	1.37
	K2	24.4	2.9	18.7	11.9	13.73	0.12	−100	0	3.45
	K1	21.8	2.2	20.6	10.1	20.03	0.22	−106	1	5.22
1215+303					*1993.15*					
	C	34.2	–	–	–	–	–	–	–	0.29
	K5	3.6	–	–	–	0.84	0.07	94	13	0.39
	K4	2.0	–	–	–	2.34	0.39	105	30	0.67
					1998.49					
	C	224.2	–	–	–	–	–	–	–	0.21
	K5	30.9	6.8	29.5	22.0	1.39	0.02	146	1	0.42
	K4	5.0	–	–	–	3.18	0.13	143	2	0.56
	K3	5.4	–	–	–	6.09	0.22	139	2	1.55
	K2	2.0	–	–	–	10.04	0.17	138	1	0.07
	K1	7.2	–	–	–	15.48	0.50	143	2	3.32
1227+255					*1998.49*					
	C	180.7	4.6	28.2	2.5	–	–	–	–	0.12
	K4	14.8	3.7	30.8	22.0	1.14	0.03	−127	2	0.23
	K3	9.9	1.5	3.1	10.6	2.35	0.05	−117	2	0.88
	K2	15.8	1.7	–76.2	22.4	4.32	0.17	−114	2	3.71
	K1	15.8	1.2	87.3	9.7	7.87	0.16	−127	1	4.09
1235+632					*1993.15*					
	C	14.1	–	–	–	–	–	–	–	0.16
	K1	1.9	–	–	–	1.74	0.12	150	5	0.19
1553+113					*1998.49*					
	C	182.9	4.2	22.8	2.3	–	–	–	–	0.24
	K4	19.0	2.8	3.3	14.7	0.68	0.03	53	3	1.07
	K3	8.9	–	–	–	3.24	0.24	20	4	3.82
	K2	4.6	–	–	–	10.02	0.92	58	7	6.22
	K1	2.4	–	–	–	97.03	1.20	85	1	5.85

Table 3 – *continued*

Source	Component	I (mJy)	p (mJy)	χ (°)	m (per cent)	r (mas)	Δr (mas)	θ (°)	$\Delta\theta$ (°)	FWHM (mas)
1727+502					*1995.53*					
	C	76.2	1.2	–1.6	1.6	–	–	–	–	0.28
	K3	26.6	1.4	44.5	5.3	1.78	0.03	−45	1	0.96
	K2	17.1	1.5	27.3	8.8	3.25	0.06	−34	1	1.59
	K1	27.2	1.0	62.1	3.7	5.89	0.22	−49	2	4.08
					1998.49					
	C	59.0	–	–	–	–	–	–	–	0.37
	K5	29.3	0.6	–60.3	2.0	1.15	0.01	−80	1	0.91
	K4	19.9	2.1	3.8	10.6	2.74	0.03	−57	1	1.08
	K3	19.8	2.3	42.9	11.6	4.67	0.03	−62	1	1.43
	K2	16.1	–	–	–	6.74	0.07	−56	1	2.48
	K1	15.6	–	–	–	15.74	0.27	−51	1	6.11
1741+196					*1998.49*					
	C	84.2	0.9	–55.0	1.1	–	–	–	–	0.38
	K6	15.9	–	–	–	1.14	0.03	73	2	0.53
	K5	14.4	1.4	–33.7	9.7	2.75	0.03	79	1	1.11
	K4	7.3	0.8	–29.9	10.9	5.87	0.11	84	2	2.23
	K3	2.1	–	–	–	9.37	0.56	84	4	2.78
	K2	1.6	–	–	–	13.39	1.79	88	7	4.37
	K1	4.5	–	–	–	19.53	1.25	95	4	7.39
1743+398					*1998.49*					
	C	47.7	0.7	54.6	1.5	–	–	–	–	0.06
	K2	7.0	–	–	–	1.60	0.07	−179	1	0.48
	K1	3.7	1.0	28.6	27.0	5.25	0.25	178	1	1.48
2201+044					*1998.49*					
	C	155.4	–	–	–	–	–	–	–	0.39
	K2	31.0	0.76	–50.9	2.5	1.19	0.04	−43	2	0.21
	K1	8.2	–	–	–	3.39	0.08	−48	1	0.74

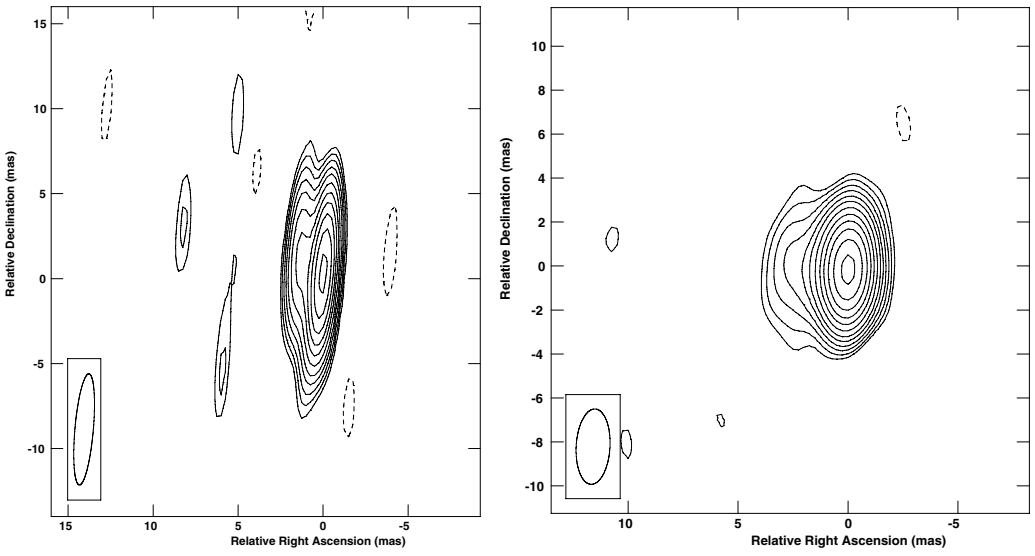

Figure 1. Total intensity image of the HBL 0414+009. Left-hand panel: Epoch 1993.15. Contours are −2.8, 2.8, 5.6, 11.2, 22.5, 45 and 90 per cent of the peak surface brightness of 27.2 mJy beam^{-1}. Right-hand panel: Epoch 1995.53. Contours are −2, 2, 2.8, 4, 5.6, 8, 11, 16, 23, 32, 45, 64, 90 per cent of the peak surface brightness of 38.6 mJy beam^{-1}.

Patnaik et al. (1992) shows only the unresolved core. The source is quite core-dominated in our VLBI image (Fig. 6), but also shows a clear jet to the south-east, well aligned with the structure observed by Giroletti et al. (2004b). The VLBI core displays the very high fractional polarization of $m_c = 15$ per cent, while no polarization was detected in the jet.

5.7 1011+496

This object has been detected in TeV γ-rays by the MAGIC telescope (Albert et. al. 2007). The 1.5-GHz VLA image of Kollgaard et al. (1996b) shows extended emission towards the west. Our VLBI image (Fig. 6) shows a VLBI jet extending towards the west.

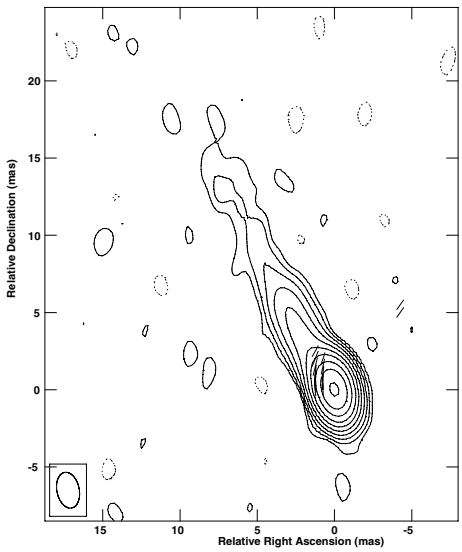

Figure 2. Total-intensity image of the HBL 0652+426, epoch 1998.49, with χ vectors superimposed. Contours are −0.17, 0.17, 0.35, 0.70, 1.40, 2.80, 5.60, 11.20, 22.50, 45 and 90 per cent of the peak surface brightness of 136.6 mJy beam^{-1}, χ vectors: 1 mas = 1 mJy beam^{-1}.

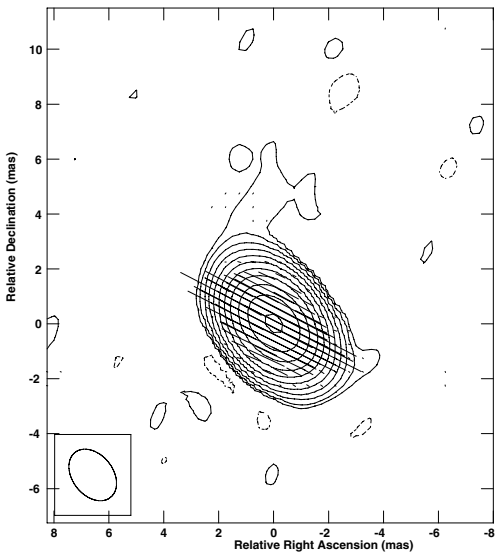

Figure 4. Total-intensity image of the LBL 0749+540, epoch 1998.49, with χ vectors superimposed. Contours are −0.09, 0.09 0.17, 0.35, 0.70, 1.40, 2.80, 5.60, 11.20, 22.50, 45 and 90 per cent of the peak surface brightness of 163.3 mJy beam^{-1}, χ vectors: 1 mas = 20 mJy beam^{-1}.

Polarization was detected in the core, inner jet, and outer jet, ∼6 mas from the core. The χ vectors imply that the *B* field is roughly aligned with the inner jet, but may become transverse in the outer jet.

5.8 1101+384

1104+382 or Mrk 421 is a well-known TeV γ-ray emitting blazar (Mushotzky et al. 1978; Schwartz et al. 1979). In the 0.5–10 keV band, this source is variable on time-scales ranging from 14 h to several days and occasionally exhibits large (by a factor of 10) X-ray outbursts characterized by a marked flattening of the spectrum (George, Warwick & Bromage 1988). The 1.4-GHz kpc-scale images of Kapahi (1979) and Ulvestad, Johnston & Weiler (1983) show extended emission towards the north-west and north-east. The 22-GHz VLBP images of Piner & Edwards (2005) and 5–22 GHz VLBP images of Charlot et al. (2006) show the VLBI jet extending to the north-west, with the dominant inferred *B* field in the inner jet being transverse to the jet, although jet regions with possibly oblique (i.e. neither aligned nor perpendicular to the jet) and longitudinal *B* fields are also visible in the images of Charlot et al. (2006). Our new VLBI images (Fig. 7) are qualitatively similar to those of Charlot et al. (2006), with the predominant jet *B* field being transverse. Our images, especially the one from 1995, also show a region of faint, extended polarization ∼15–20 mas from the core, with the χ vectors being roughly aligned with the direction back towards

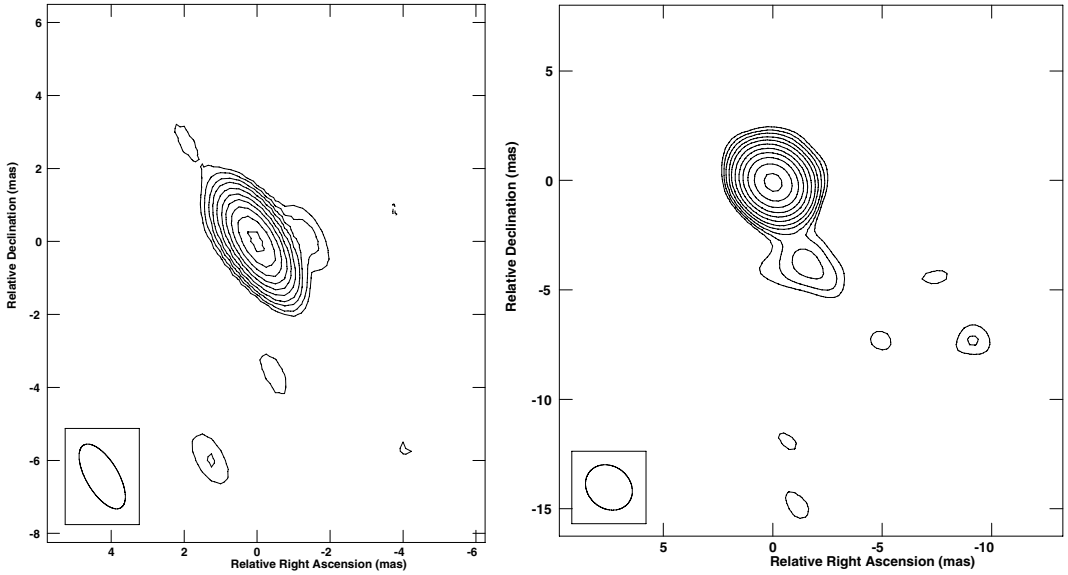

Figure 3. Total intensity images of the HBL 0706+592. Left-hand panel: Epoch 1993.15. Contours are −4, 4, 5.6, 8, 11, 16, 23, 32, 45, 64, 90 per cent of the peak surface brightness of 23.9 mJy beam^{-1}. Right-hand panel: Epoch 1995.53. Contours are −2.8, 2.8, 4, 5.6, 8, 11, 16, 23, 32, 45, 64, 90 per cent of the peak surface brightness of 27.5 mJy beam^{-1}.

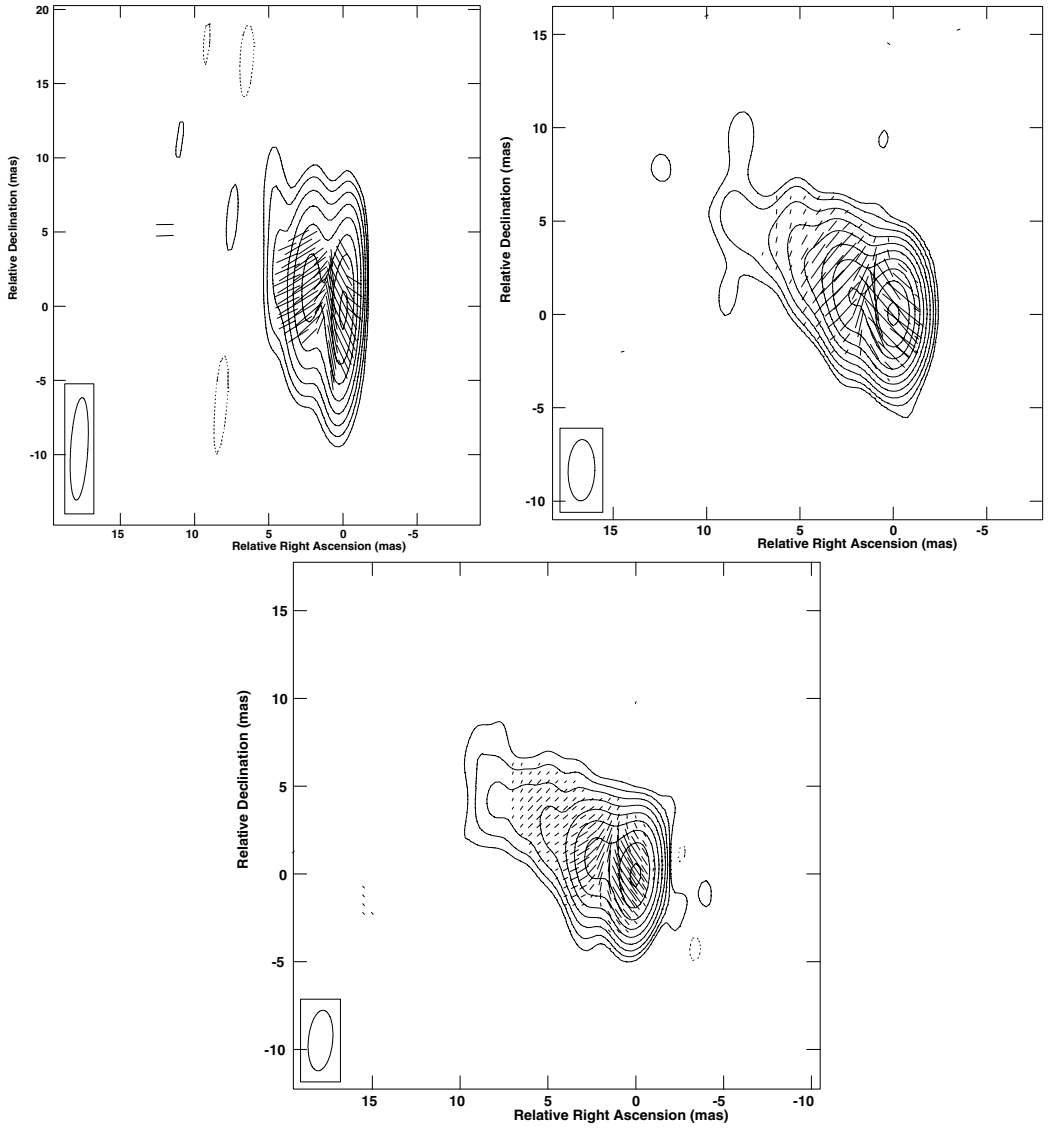

Figure 5. Total-intensity images of the LBL 0829+046 with χ vectors superimposed. Top left-hand panel: Epoch 1993.15. Contours are -0.70, 0.70, 1.40, 2.80, 5.60, 11.20, 22.50, 45 and 90 per cent of the peak brightness of 469 mJy beam^{-1}, χ vectors: 1 mas = 4 mJy beam^{-1}. Top right-hand panel: Epoch 1995.53. Contours are -0.2, 0.2, 0.35, 0.70, 1.40, 2.80, 5.60, 11.20, 22.50, 45 and 90 per cent of the peak brightness of 699.3 mJy beam^{-1}, χ vectors: 1 mas = 5 mJy beam^{-1}. Bottom panel: Epoch 1998.49. Contours are -0.35, 0.35, 0.70, 1.40, 2.80, 5.60, 11.20, 22.50, 45 and 90 per cent of the peak surface brightness of 441 mJy beam^{-1}, χ vectors: 1 mas = 8 mJy beam^{-1}.

the core; precisely the same structure is visible in the images of Charlot et al. (2006), particularly the one for 1998 March 28. This suggests that the observed total-intensity emission may represent only the edge of a much broader flow whose *B* field is transverse to the flow direction, as would be expected if we are seeing the transverse component of a toroidal or helical *B* field associated with the jet. Overall, the variations in the polarizations of individual components are appreciable, but not dramatic, being comparable to the 5-GHz polarization variations observed on similar time-scales for individual VLBI components in LBLs (e.g. Gabuzda et al. 1994).

5.9 1133+704

1133+704 is associated with the giant elliptical galaxy Mrk 180. X-ray emission was detected by the *Einstein* and *HEAO-1* observatories (Hutter & Mufson 1980), and the object is a candidate TeV BL Lac (Costamante & Ghisellini 2002). The kpc-scale radio structure has an asymmetric core–halo morphology (Antonucci & Ulvestad 1985; Laurent-Muehleisen et al. 1993; Giroletti et al. 2004b). The previous global VLBI observations of Kollgaard et al. (1996a) show a jet to the south-east. A high degree of polarization was found in the inner jet, but with the corresponding χ vectors bearing no obvious relationship to the jet direction. Our new VLBI image (Fig. 8) reveals polarized emission in both the core and jet, with the predominant implied *B* field being longitudinal. We also detect a region of polarization at the southern edge of the jet with $\chi \simeq 45^{\circ}$, whose origin is not clear.

5.10 1147+245

This source has two remarkable properties that are quite unusual for BL Lac objects: the radio structure at 1.4 GHz consists of a classical triple source (Antonucci & Ulvestad 1985), and the optical

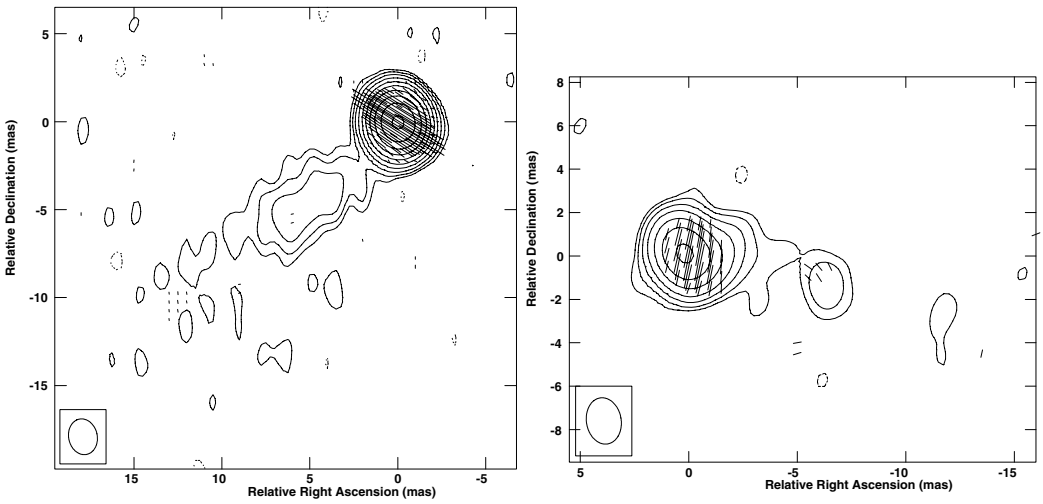

Figure 6. Total-intensity images with χ vectors superimposed. Left-hand panel: The LBL 0925+504, epoch 1998.49. Contours are −0.17, 0.17, 0.35, 0.70, 1.40, 2.80, 5.60, 11.20, 22.50, 45 and 90 per cent of the peak brightness of 433.3 mJy beam^{-1}, χ vectors: 1 mas = 10 mJy beam^{-1}. Right-hand panel: The HBL 1011+496, epoch 1998.49. Contours are −1.4, 1.40, 2.80, 5.60, 11.20, 22.50, 45 and 90 per cent of the peak brightness of 93.8 mJy beam^{-1}, χ vectors: 1 mas = 3 mJy beam^{-1}.

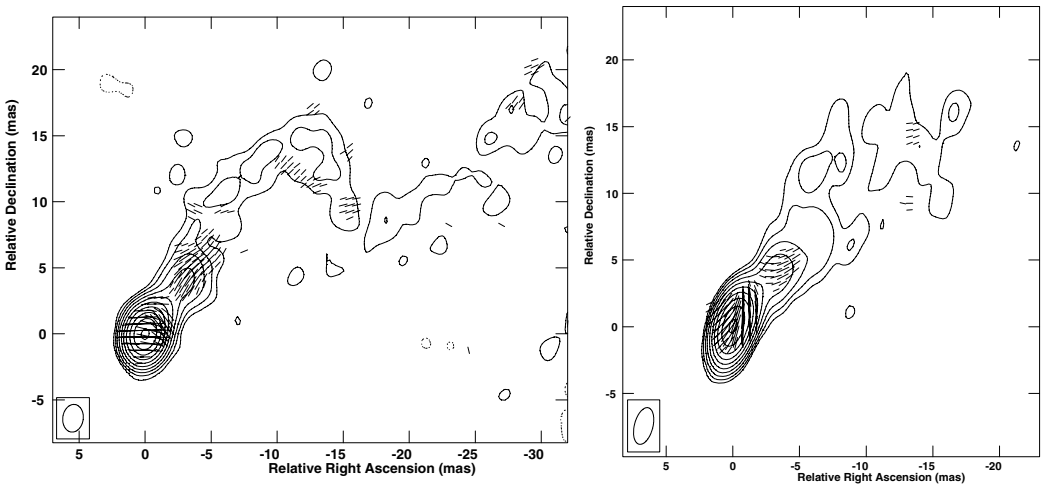

Figure 7. Total-intensity images of the HBL 1101+384 (Mrk 421) with χ vectors superimposed. Left-hand panel: Epoch 1995.53. Contours are −0.17, 0.17, 0.35, 0.70, 1.40, 2.80, 5.70, 11.50, 22.50, 45 and 90 per cent of the peak surface brightness of 326 mJy beam^{-1}, χ vectors: 1 mas = 0.9 mJy beam^{-1}. Right-hand panel: Epoch 1998.5. Contours are −0.17, 0.17, 0.35, 0.70, 1.40, 2.80, 5.70, 11.50, 22.50, 45 and 90 per cent of the peak surface brightness of 356.5 mJy beam^{-1}, χ vectors: 1 mas = 1.8 mJy beam^{-1}.

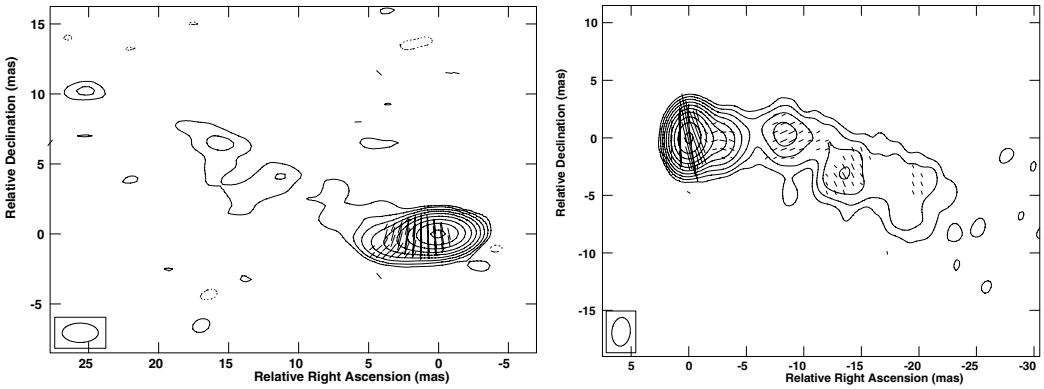

Figure 8. Total-intensity images with χ vectors superimposed. Left-hand panel: The HBL 1133+704, epoch 1998.49. Contours are −0.35, 0.35, 0.70, 1.40, 2.80, 5.70, 11.50, 22.50, 45 and 90 per cent of the peak surface brightness of 98 mJy beam^{-1}, χ vectors: 1 mas = 1.7 mJy beam^{-1}. Right-hand panel: The LBL 1147+245, epoch 1995.53. Contours are −0.17, 0.17, 0.35, 0.70, 1.40, 2.80, 5.6, 11, 23, 45 and 90 per cent of the peak surface brightness of 479.4 mJy beam^{-1}, χ vectors: 1 mas = 2.5 mJy beam^{-1}.

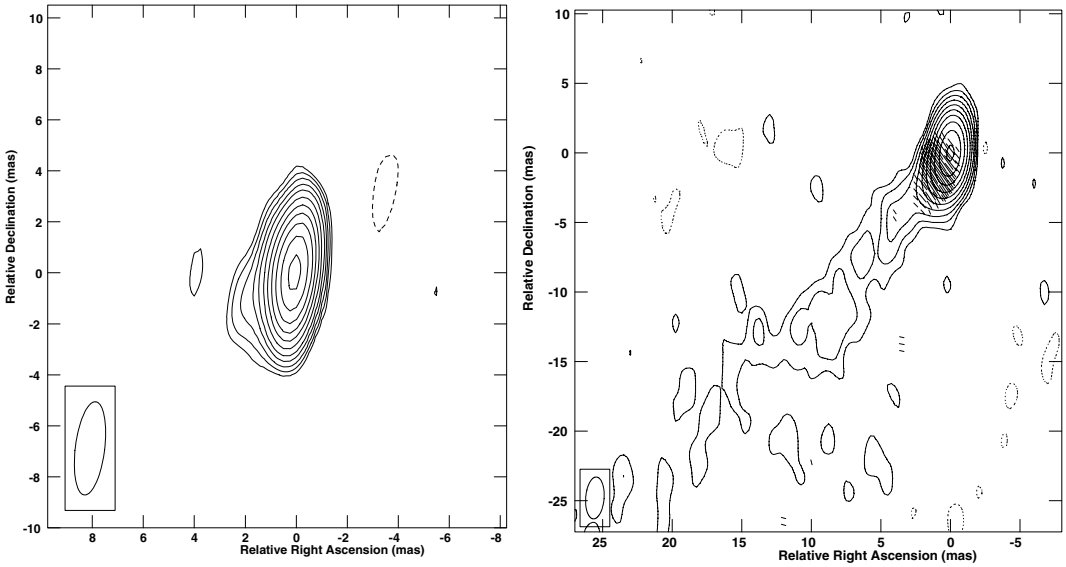

Figure 9. Total-intensity images of the HBL 1215+303 with χ vectors superimposed. Left-hand panel: Epoch 1993.15 (no polarization detected). Contours are -2.8, 2.8, 4.0, 5.6, 8, 11, 16, 23, 32, 45, 64 and 90 per cent of the peak surface brightness of 33.4 mJy beam^{-1}. Right-hand panel: Epoch 1998.49. Contours are -0.17, 0.17, 0.35, 0.70, 1.40, 2.80, 5.70, 11.50, 22.50, 45 and 90 per cent of the peak surface brightness of 231 mJy beam^{-1}, χ vectors: 1 mas = 2 mJy beam^{-1}.

variability is rather small, with a total amplitude of only 0.77 mag (Pica et al. 1988). The kpc-scale radio emission extends roughly in the north–south direction. The previous 5-GHz VLBP image of Gabuzda, Pushkarev & Cawthorne (1999) shows the VLBI jet extending to the west, misaligned with the large-scale structure. Only weak polarization was detected from the jet, corresponding to a transverse *B* field. In our new VLBI image (Fig. 8), polarization is detected throughout the jet, with the χ vectors in the inner jet at and beyond $\sim$15 mas from the core being aligned with the jet, indicating transverse *B* fields. The relative orientation of the χ vectors in another region of polarization $\sim$8 mas from the core is not clear.

5.11 1215+303

The 1.5-GHz VLA image of Laurent-Muehleisen et al. (1993) shows an unresolved core with a hint of extended emission towards the south-west. The core-to-lobe ratio is $\geqslant$14, the largest in the *HEAO-1* sample. Our 1993 image shows a short jet in PA $\sim$ 135°, and our 1998 image reveals a well-defined straight jet in this same PA (Fig. 9). Polarization was detected only at the latter epoch, in both the core and inner jet. The inferred jet *B* field is aligned with the jet. The jet component K5 was roughly 22 per cent polarized at epoch 1998.49, when the total intensity of this feature was about a factor of 8 higher than at our earlier epoch, 1993.15. If K5 were comparably polarized in 1993.15, it would have had a polarized flux of only about 0.7–0.8 mJy, making the absence of a polarization detection at the earlier epoch unsurprising.

5.12 1227+255

This BL Lac object was identified during the correlation of the RASS with the Hamburg Quasar Survey (Nass et al. 1996). Our VLBI image (Fig. 10) shows a jet that initially emerges to the south-west, then curves towards the south. Polarization was detected in both the pc-scale core and jet. The χ vectors in the inner jet are roughly aligned with the jet direction, implying a transverse *B* field, and a 'sheath' of longitudinal *B* field is observed along the northern edge of the jet, where the jet appears to be bending.

5.13 1235+632

The 1.5-GHz VLA image of Laurent-Muehleisen et al. (1993) does not reveal any extended structure. Our VLBI image (Fig. 10) shows a pc-scale jet extending in PA $\sim$ 140°. No polarization was detected.

5.14 1553+113

The 1.4-GHz VLA image of Rector et al. (2003a) shows a faint lobe south of the core, with a weak 'hotspot' in PA = 160°. The 5-GHz VLBA map however shows a jet extending to the north-east in PA = 48°, giving a large misalignment of ΔPA = 112° (Rector et al. 2003a). Our VLBI map (Fig. 11) shows a dominant core and a short jet in PA $\sim$ 45°. There may be fainter jet emission further from the core in this same direction, and also possibly a faint extension on the counterjet side. Polarization was detected in both the core and inner jet, but the orientation of the χ vectors relative to the jet is unclear.

5.15 1727+502

1727+502 is a candidate TeV BL Lac (Costamante & Ghisellini 2002). The kpc-scale radio structure consists of an unresolved core and diffuse, asymmetrical halo, with evidence for a jet emerging to the north-west (Wardle, Moore & Angel 1984b; Giroletti et al. 2004b). The previous 5-GHz VLBP image of Kollgaard et al. (1996a) show a jet extending to the north-west, roughly aligned with the kpc-scale structure. Polarization was detected in several jet components, with the implied *B* field being either transverse or longitudinal in the inner jet, depending on interpretation, then becoming clearly longitudinal further from the core. Our new VLBI images (Fig. 12) clearly show regions of polarization corresponding to longitudinal *B* fields offset from the jet ridge line, forming a sort

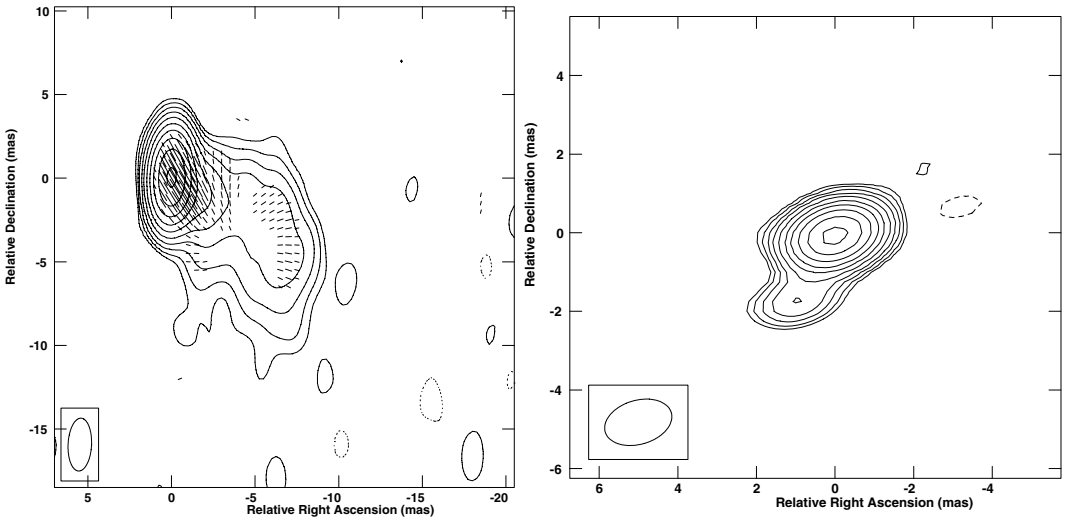

Figure 10. Total-intensity images with χ vectors superimposed. Left-hand panel: The HBL 1227+255, epoch 1998.49. Contours are −0.17, 0.17, 0.35, 0.70, 1.40, 2.80, 5.60, 11.20, 22.50, 45 and 90 per cent of the peak surface brightness of 183.7 mJy beam^{-1}, χ vectors: 1 mas = 2.5 mJy beam^{-1}. Right-hand panel: The HBL 1235+632, epoch 1993.15 (no polarization detected). Contours are −4, 4, 5.6, 8, 11, 16, 23, 32, 45, 64, 90 per cent of the peak surface brightness of 13.8 mJy beam^{-1}.

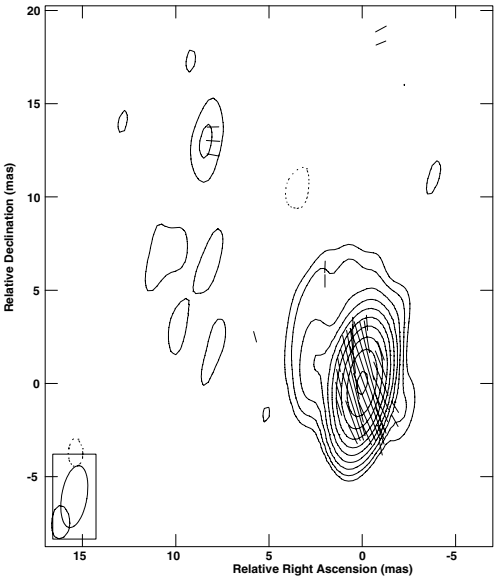

Figure 11. Total-intensity image of the LBL 1553+113, epoch 1998.49, with χ vectors superimposed. Contours are −0.19, 0.19, 0.35, 0.70, 1.40, 2.80, 5.60, 11, 23, 45 and 90 per cent of the peak surface brightness of 189.7 mJy beam^{-1}, χ vectors: 1 mas = 1.5 mJy beam^{-1}.

of 'sheath' of polarization. The 1998 image also shows a region of transverse *B* field in the inner jet, thus overall a 'spine-sheath'-like polarization structure. There were no dramatic changes in the polarization properties of individual VLBI components in the roughly three years between our two epochs.

5.16 1741+196

VLA snapshot observations of this source (see Perlman et al. 1996) show a jet in PA $\sim 90^\circ$. The 5-GHz VLBA image of Rector et al. (2003a) shows a collimated straight jet extending to the east in PA $= 86^\circ$, well aligned with the VLA jet. Our VLBI map (Fig. 13) clearly shows a well-defined straight jet extending in PA $\sim 90^\circ$. Polarization was detected in the core and two jet components, but the χ vectors bear no obvious relationship to the direction of the jet structure.

5.17 1743+398

This BL Lac object lies close to the centre of a moderately massive galaxy cluster (Nilsson et al. 1999). The 1.4-GHz VLA image of this source shows a highly distorted FR I morphology; the jets lie in the north-west and south-east directions, and show sharp bends (Rector, Gabuzda & Stocke 2003b). Our VLBI image (Fig. 13) shows a jet pointing nearly to the south. There is evidence for a 'sheath' of longitudinal *B* field at the eastern edge of the jet.

5.18 2201+044

Many radio observations have mapped the intricate extended structure in this Seyfert 1 galaxy at different frequencies and resolutions (Ulvestad & Johnston 1984; van Gorkom et al. 1989). The 1.5-GHz observations of Laurent-Muehleisen et al. (1993) revealed a broad jet extending towards the north-west in PA $\sim -50^\circ$ and faint extended emission to the east. The previous VLBI image of Kollgaard et al. (1996a) showed a compact jet structure in PA $\sim -42^\circ$, aligned with the dominant kpc-sale structure; no pc-scale polarization was detected. Our new VLBI map (Fig. 14) shows a jet in the same PA, i.e. $\sim -40^\circ$. Polarization was detected only in the jet, with the inferred *B* field being perpendicular to the jet direction.

6 VLBI PROPERTIES OF LBLS AND HBLs AT 6 cm

The data for the LBLs, which belong primarily to the 1-Jy sample (Kühr & Schmidt 1990), have been obtained from Gabuzda et al. (2000). Data for four additional LBLs belonging to our *HEAO-1* + RGB sample have been included in the analysis. Of these, 1147+245 also belongs to the 1-Jy sample. The data for the HBLs come primarily from our *HEAO-1* + RGB sample. The redshift and

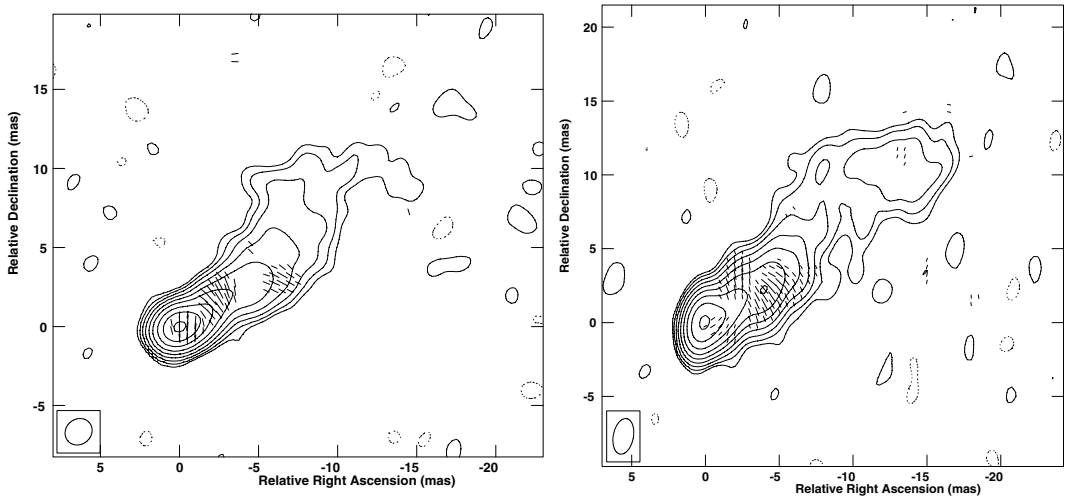

Figure 12. Total intensity image of the HBL 1727+502 with χ vectors superimposed. Left-hand panel: Epoch 1995.53. Contours are −0.35, 0.35, 0.70, 1.40, 2.80, 5.60, 11, 23, 45 and 90 per cent of the peak surface brightness of 77.2 mJy beam^{-1}, χ vectors: 1 mas = 1 mJy beam^{-1}. Right-hand panel: Epoch 1998.49. Contours are −0.35, 0.35, 0.70, 1.40, 2.80, 5.60, 11.20, 22.50, 45 and 90 per cent of the peak brightness of 64.2 mJy beam^{-1}, χ vectors: 1 mas = 1.8 mJy beam^{-1}.

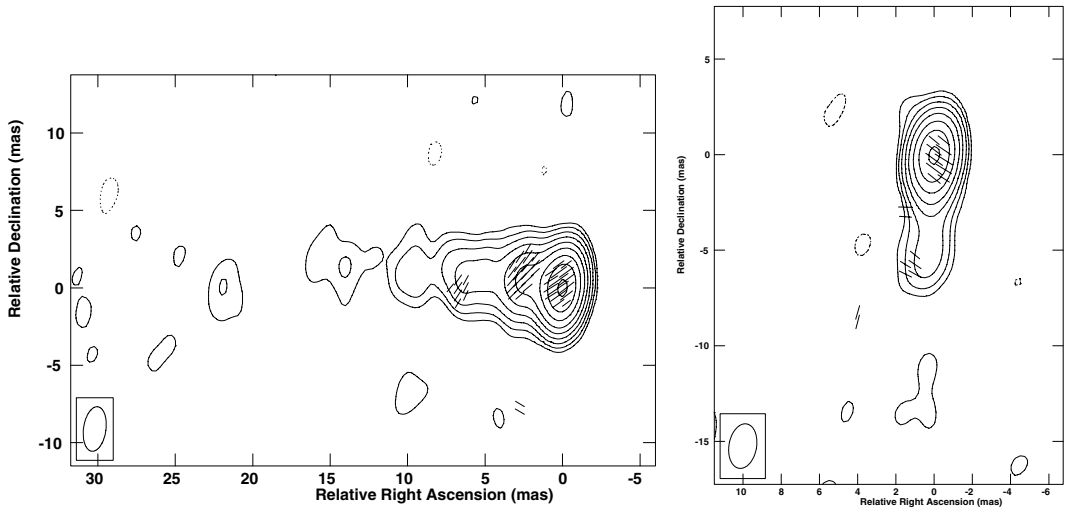

Figure 13. Total-intensity images with χ vectors superimposed. Left-hand panel: The HBL 1741+196, epoch 1998.49, Contours are −0.35, 0.35, 0.70, 1.40, 2.80, 5.60, 11.20, 22.50, 45 and 90 per cent of the peak surface brightness of 84.3 mJy beam^{-1}, χ vectors: 1 mas = 1.3 mJy beam^{-1}. Right-hand panel: The HBL 1743+398, epoch 1998.49. Contours are −0.70, 0.70, 1.40, 2.80, 5.60, 11, 23, 45 and 90 per cent of the peak surface brightness of 49.3 mJy beam^{-1}, χ vectors: 1 mas = 0.9 mJy beam^{-1}.

1.4-GHz radio power distributions for the LBL and HBL samples are presented in Figs 15 and 16, respectively. The distributions of the core fractional polarization, the inner jet ($r < 10$ pc from the core) fractional polarization, the difference between the core polarization angle and the jet direction $|\chi_c - \theta|$ and the difference between the inner jet polarization angle and the jet direction $|\chi_j - \theta|$ for LBLs and HBLs are presented in Figs 17–20, respectively. Table 4 tabulates the values for these parameters. Note that multiple values for a single source are included in the histograms if they fall in different bins, but not if they fall in the same bin. The Seyfert 1 galaxy 2201+044 was excluded from the analysis.

Table 6 summarizes the results of the comparison between LBLs and HBLs. It has the following columns. Column 1: the property being compared; column 2: the corresponding two-sided Kolmogorov–Smirnov (KS) statistic, which specifies here the maximum deviation between the cumulative distributions for the LBLs and HBLs; column 3: the significance level of the KS statistic, i.e. the probability that the cumulative distributions for the LBLs and HBLs are intrinsically similar; column 4: 'YES' and 'NO' indicate if the differences between the properties of the two BL Lac populations are statistically significant or not, while YES? indicates a difference that is significant at the 2σ level.

6.1 Parsec-scale core polarization

We have detected pc-scale polarized emission in all but three of the HBLs in our *HEAO-1* + RGB sample. We find that the degree of polarization in the core, m_c, is typically less than 3 per cent in the HBLs, with only one HBL (1011+496) having $m_c \geqslant 4$ per cent (see Fig. 17). On the other hand, LBLs typically have $m_c > 3$ per cent

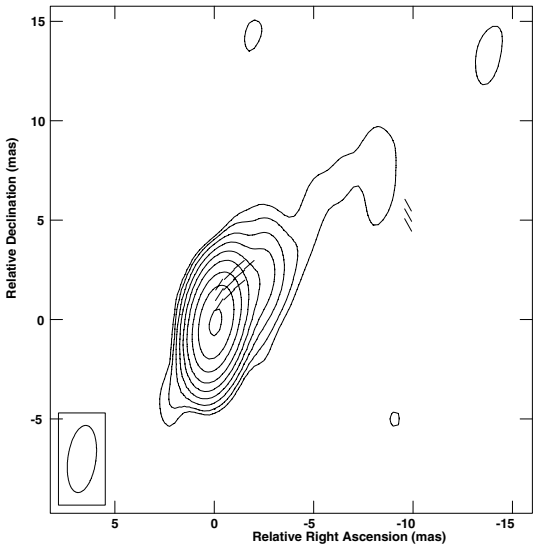

Figure 14. Total-intensity images of the Seyfert 1 2201+044, epoch 1998.49, with χ vectors superimposed. Contours are −0.4, 0.4, 0.70, 1.40, 2.80, 5.60, 11, 23, 45 and 90 per cent of the peak surface brightness of 162.3 mJy beam^{-1}, χ vectors: 1 mas = 0.9 mJy beam^{-1}.

with the core polarizations occasionally exceeding 10 per cent (Fig. 17). It is interesting that two of the X-ray-selected BL Lac objects for which results are presented here have among the highest core fractional polarizations ever measured –0749+540 ($m_c \sim$ 9 per cent) and 0925+504 ($m_c \sim 15$ per cent); however, these prove to be LBLs, so that their core fractional polarizations fall within the previously observed range for this class.

A two-sided KS test on the distribution of m_c for the HBL and LBL subclasses indicates only a 0.3 per cent probability that the two data sets come from the same parent population (Table 6). The tendency for the LBLs to have higher pc-scale core fractional polarization than the HBLs has also been observed in the kpc-scale cores of these BL Lac objects (Kollgaard et al. 1996a). Although both LBLs and HBLs have relatively modest redshifts compared to the quasars, there is a significant difference in the redshift distribution of LBLs and HBLs (Fig. 15). The KS test indicates that the probability that the two data sets come from the same parent population is only around 0.02 per cent (Table 6). This would result in the VLBI observations probing somewhat different spatial scales in the two BL Lac subclasses. Therefore there is a possibility that, on average, the radio cores of LBLs include greater contributions from the inner radio jets than do the radio cores of HBLs, resulting in higher average core fractional polarizations. However, when we tested this we did not find any correlation between core fractional polarization and redshift for the LBLs (Spearman rank test; $p = 0.9$). Further, this idea could not simultaneously explain the origin of the lower core fractional polarizations in quasars compared to LBLs (Gabuzda et al. 2000), since quasars tend to typically have *higher* redshifts than BL Lac objects. Based on significant differences in the total and extended power, as discussed later in Section 7, we infer the low m_c in HBLs to be due to their intrinsically weaker radio cores.

We find that the polarization-angle orientations in the pc-scale cores relative to the inner VLBI jet direction are not statistically significantly different in HBLs and LBLs (see Fig. 18 and Table 6). However, while in LBLs there is a clear tendency for χ_c to lie either parallel or perpendicular to the jet direction (see Gabuzda et al. 2000), such a behaviour is not observed in HBLs. Optical depth effects as discussed by Gabuzda (2003) could however be contributing to the differences in the observed EVPA distributions.

6.2 Parsec-scale jet polarization

Fig. 19 shows the distribution of the inner jet fractional polarizations for LBLs and HBLs. The range of fractional polarizations in the inner jets (say, within 10 pc from the core), m_j, is the same for LBLs and HBLs, with the highest jet polarizations in both classes reaching tens of per cent, indicating the presence of highly aligned B fields. The KS test on the m_j distributions for the HBLs and LBLs indicates a ∼74 per cent probability that the two data sets come from the same parent population (Table 6).

However, the jet polarization-angle orientation displays an intriguing difference between HBLs and LBLs. While the jet EVPAs are predominantly aligned with the VLBI jet direction in LBLs, the EVPAs in HBLs show a tendency to be greater than 60° with respect to the jet direction, that is, roughly perpendicular to the local jet direction (Fig. 20). The KS test indicates a difference in the jet EVPAs between HBLs and LBLs at the ∼93 per cent significance level. Assuming that the jet emission is optically thin, this result if true for HBLs, implies that the HBLs show predominantly longitudinal jet B fields, while the LBLs possess predominantly transverse jet B fields. Clearly this bimodality in B field structure needs to be tested with a larger sample of HBLs. We note that the jet EVPAs

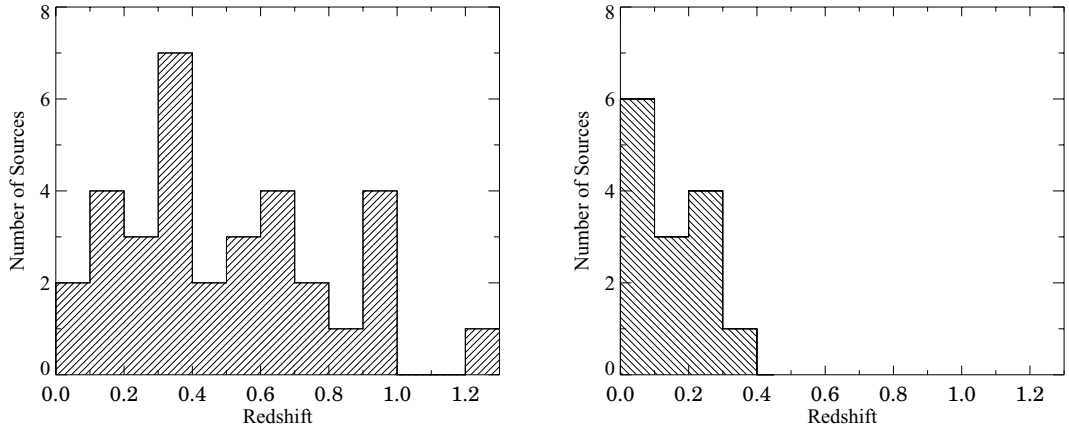

Figure 15. The redshift distributions of LBLs (left-hand panel) and HBLs (right-hand panel). The LBLs are primarily 1-Jy BL Lacs Gabuzda et al. (2000) but include four LBLs from our *HEAO-1* + RGB sample while the HBLs belong to our *HEAO-1* + RGB sample and include Mrk 501 from the 1-Jy sample.

Table 4. HBL core and jet polarization properties.

Source	m_c (per cent)	m_j [jet component] (per cent)	$\|\chi_c - \theta\|$ (°)	$\|\chi_j - \theta\|$ [jet component] (°)
0414+009	–	–	–	–
0652+426	–	3.8	–	42
0706+592	–	–	–	–
0749+540	9.7	–	–	–
0829+046	3.2	4.0 [K4], 5.8 [K3]	30	50 [K4], 80 [K3]
	2.9	6.1 [K5], 5.9 [K4]	3	51 [K5], 88 [K4]
	4.4	10.9 [K6], 4.9 [K5]	21	62 [K6], 65 [K5]
0925+504	14.2	–	69	–
1011+496	4.7	3.5	82	80
1101+384	1.5	7.7 [K8], 27.2 [K6]	55	55 [K8], 6 [K6]
	1.2	15.4 [K5], 9.8 [K3]	14	37 [K5], 30 [K3]
1133+704	–	28.6 [K6], 14.5 [K5]	–	81 [K6], 34 [K5]
1147+245	4.3	5.3	73	12
1215+303	–	22.0	–	64
1227+255	2.5	22.0 [K4], 10.6 [K3]	25	22 [K4], 60 [K3]
1553+113	2.3	14.7	30	50
1727+502	1.6	5.3 [K3], 8.8 [K2], 3.7 [K1]	43	90 [K3], 61 [K2], 69 [K1]
	–	2.0 [K5], 10.6 [K4], 11.6 [K3]	–	20 [K5], 61 [K4], 75 [K3]
1741+196	1.1	9.7 [K5], 10.9 [K4]	52	67 [K5], 66 [K4]
1743+398	1.5	–	54	–
2201+044	–	2.5	–	8

Notes: 0829+046: there is an extended region with inferred longitudinal *B*-field further from the core. 1101+384: clear evidence for extended regions with *B*-field perpendicular to the jet direction slightly further from the core. 1147+245: the inferred *B*-field appears to remain perpendicular to the local jet direction further from the core as the jet bends. 1227+255: evidence for a sheath of longitudinal *B*-field further from the core. 1727+502: evidence for a sheath of longitudinal *B*-field at edges of the jet.

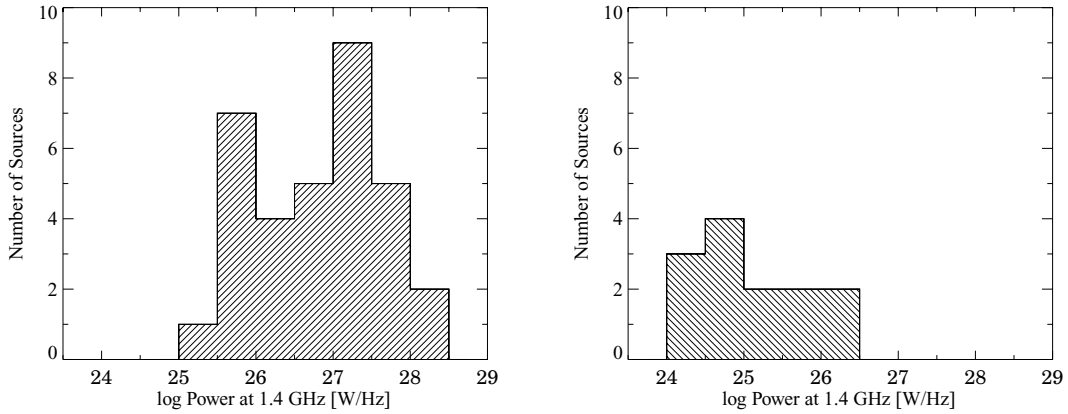

Figure 16. The total radio power at 1.4 GHz for LBLs (left-hand panel) and HBLs (right-hand panel). The LBLs are primarily 1-Jy BL Lacs Gabuzda et al. (2000) but include three LBLs from our *HEAO-1* + RGB sample while the HBLs belong to our *HEAO-1* + RGB sample and include Mrk 501 from the 1-Jy sample. The 1.4-GHz radio data were obtained from the NASA/IPAC Extragalactic Database (NED).

of those HBLs which have alternatively been classified as IBLs by Nieppola, Tornikoski & Valtaoja (2006), occupy the middle of the EVPA range (between 20° and 70°). This behaviour also warrants further investigation.

Some of the HBLs show evidence for a 'spine-sheath' *B* field structure, with the inner region of the jet having transverse *B* fields and the edges having longitudinal *B* fields. This type of *B* field structure has been observed in other blazars (Attridge, Roberts & Wardle 1999; Giroletti et al. 2004a) and it could result from interaction of the jet with the surrounding medium, or due to jet acceleration being a function of the angular distance from the jet axis, producing a velocity structure (Ghisellini, Tavecchio & Chiaberge 2005). Alternatively, as Gabuzda, Murray & Cronin (2004) and Lyutikov, Pariev & Gabuzda (2005) have pointed out, this could be associated with the presence of a helical *B* field associated with the jets of these objects. Such fields could come about in a natural way due to the 'winding up' of a seed field via the combination of outflow and rotation of the central black hole–accretion disc system. Particularly good examples of a 'spine-sheath' *B* field structure are 1227+255 (Fig. 10) and 1727+502 (Fig. 12).

6.3 Apparent speeds

We were able to derive tentative two-epoch apparent speeds for a number of the objects in our sample from the model-fitting re-

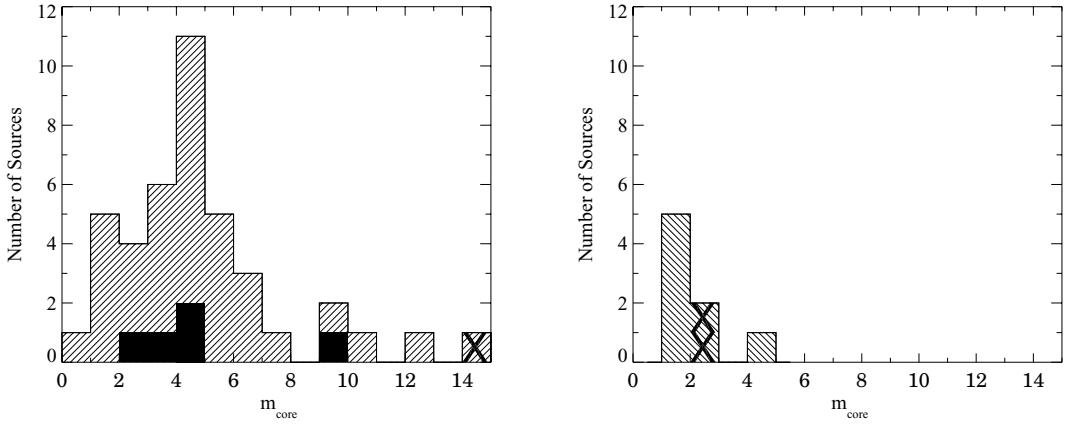

Figure 17. Distributions of core fractional polarization for the 1-Jy LBLs (left-hand panel) and HBLs (right-hand panel). The shaded regions mark the LBLs belonging to our *HEAO-1* + RGB sample. X denotes a BL Lac that is alternately classified as an IBL by Nieppola et al. (2006).

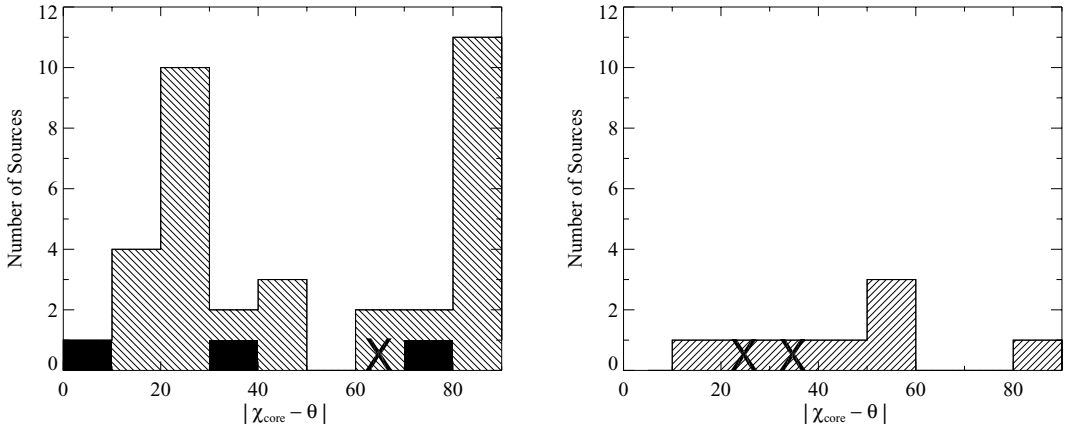

Figure 18. Distributions of offset between the core polarization angle χ_c and the direction of the VLBI jet for the 1-Jy LBLs (left-hand panel) and HBLs (right-hand panel). The distribution is bimodal for LBLs with preferred values close to 0° and 90°, while the HBLs seem to show the whole range of angles. The shaded regions mark the LBLs belonging to our *HEAO-1* + RGB sample. X denotes a BL Lac that is alternately classified as an IBL by Nieppola et al. (2006).

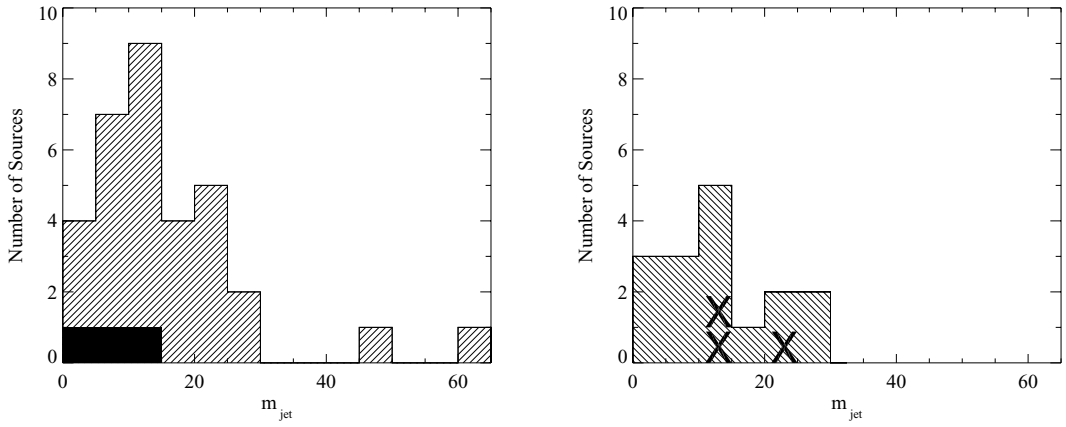

Figure 19. Distributions of inner jet ($r < 10$ pc) fractional polarization for LBLs (left-hand panel) and HBLs (right-hand panel). The shaded regions mark the LBLs belonging to our *HEAO-1* + RGB sample. X denotes a BL Lac that is alternately classified as an IBL by Nieppola et al. (2006).

sults in Table 3, either on their own or combined with results from the literature. We also derived firmer speeds for a smaller number of objects based on three or more epochs, by combining our results with other model fits in the literature. The collected apparent speeds for these and other HBLs from the literature are tabulated in Table 5, where column 3 gives the jet component speeds, and column 4 the number of epochs used for estimating these speeds.

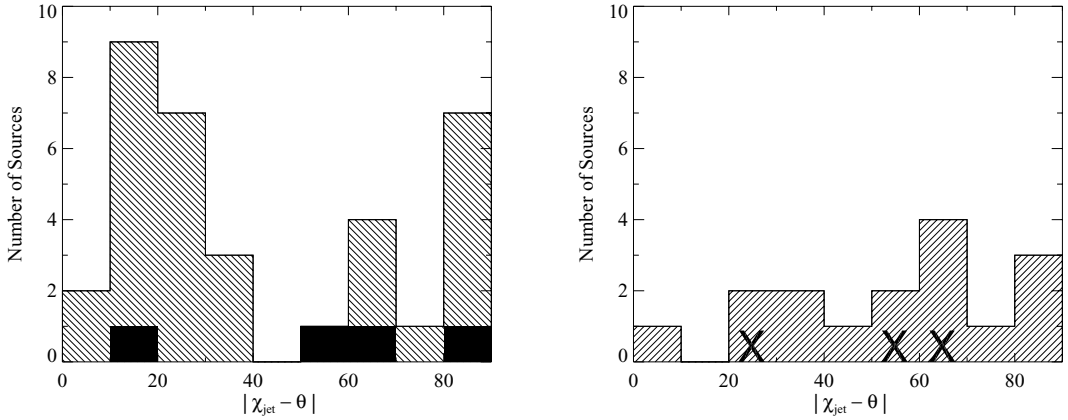

Figure 20. Distributions of offset between the inner jet ($r < 10$ pc) polarization angle χ_j and the direction of the VLBI jet for LBLs (left-hand panel) and HBLs (right-hand panel). The LBL distribution shows a predominance of values close to 0° and a secondary peak near 90°. The HBL distribution shows a large range of angles with a predominance of values larger than 60°. The shaded regions mark the LBLs belonging to our *HEAO-1* + RGB sample. X denotes a BL Lac that is alternately classified as an IBL by Nieppola et al. (2006).

Table 5. Apparent speeds.

Source	Proper motion (mas yr^{-1})	β_{app}	Number of epochs	Reference
0414+009	0.13	1.81	2	P
0829+046	0.52, 0.54, 0.62, 0.88	4.95, 5.14, 5.90, 8.37	3	P
1101+384	0.02, 0.03, 0.04, 0.05	0.03, 0.06, 0.09, 0.10	28	PE05
1133+704	0.04, 0.18, 0.78	0.11, 0.51, 2.23	4	W
1215+303	0.10, 0.16	0.75, 1.19	2	P
1652+398	0.12, 0.25	0.26, 0.54	12	EP02, PE04
1727+502	0.03, 0.16, 0.47, 1.53	0.10, 0.55, 1.63, 5.30	6, 6, 6, 5	W
1741+196	0.04, 0.23	0.20, 1.17	5, 6	W
2155−304	0.117	4.37	3	PE04
2344+514	0.044	1.15	4	PE04

Notes: Reference for component speeds – P = present work, EP02 = Edwards & Piner (2002), PE04 = Piner & Edwards (2004), PE05 = Piner & Edwards (2005), W = Wu et al. (2007).

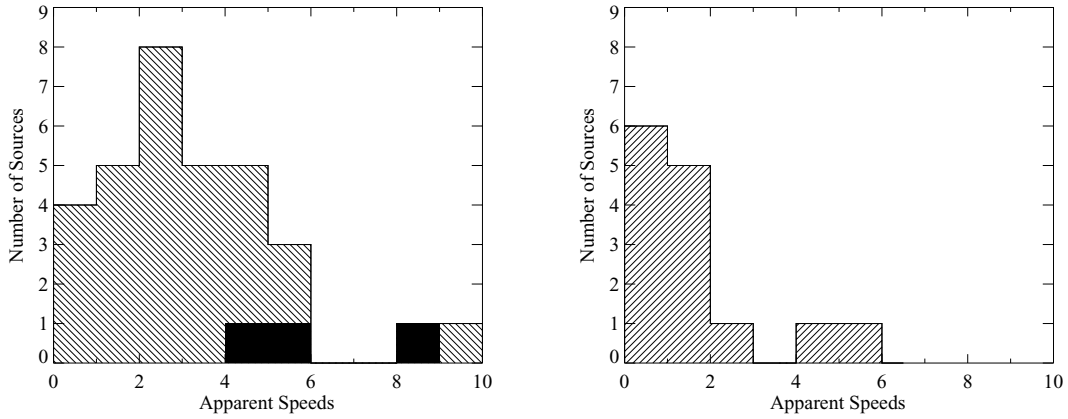

Figure 21. Distribution of apparent speeds of the jet components for the 1-Jy LBLs (left-hand panel) and the HBLs (right-hand panel). The apparent speeds in the LBLs show a peak between 2c and 3c, somewhat higher than the peak of 1c– 2c seen in our HBLs. The shaded regions mark the LBLs belonging to our *HEAO-1* + RGB sample.

LBLs typically show superluminal motions with apparent speeds in the range 1c– 5c (Gabuzda et al. 2000). In Fig. 21 we have plotted the apparent speeds of these, along with the LBL 0829+046 from the *HEAO-1* sample, shaded in black, which exhibits component speeds of ≈5c. Fig. 21 also shows the distribution of apparent speeds for our HBL sample. We find that β_{app} is typically less than 2 for the HBLs. A two-sided KS test indicates that the HBL and LBL speeds are different at the 99.9 per cent significance level. This

Table 6. The KS test statistic and probability for various parameters for HBLs and LBLs.

Parameter	KS statistic	Probability	Significantly different?
$L_{1.4}$	0.755	1.57E−05	YES
z	0.655	0.000 18	YES
$m_{\rm core}$	0.655	0.003	YES
$\beta_{\rm app}$	0.589	0.001	YES
$\|\chi_{\rm j} - \theta\|$	0.371	0.074	YES?
$\|\chi_{\rm c} - \theta\|$	0.319	0.436	NO
$m_{\rm jet}$	0.198	0.738	NO

could suggest that either the HBL jets have lower Lorentz factors compared to LBLs, or they are oriented at larger angles to the line of sight.

7 DISCUSSION

7.1 Nature of the core polarization

The HBL VLBI cores show lower fractional polarizations than LBL cores. The lack of a correlation between core fractional polarization and redshift at a high significance level however, suggests that the higher $m_{\rm c}$ values may be inherent to LBLs, and is not merely a resolution effect due to their higher average redshifts. There exists a possibility that the characteristic optical depths of the HBL cores are higher than those of the LBL cores, leading to lower observed $m_{\rm c}$ values for the HBLs. In this case, we might expect to observe different behaviour in the distributions of $\chi_{\rm c}$ for the HBLs and LBLs, which is observed in Fig. 18 albeit for a very small number of sources. However, it appears that the HBL cores could be intrinsically less luminous than LBLs, as also suggested by Giommi & Padovani (1994) and Padovani & Giommi (1995). Fig. 16 and Table 6 demonstrate that HBLs are less luminous in their total radio emission, while Urry & Padovani (1995) have shown that the same is true for their extended emission, supporting the picture wherein the radio cores in HBLs are intrinsically weaker than in LBLs.

7.2 Jet polarization in HBLs and other core-dominated AGN

7.2.1 Differences in viewing angles

Although larger viewing angles in HBLs were initially invoked to explain their less extreme radio properties, this hypothesis was brought into question when the HBL/LBL SEDs could not be reconciled simply with different viewing angles. This debate is currently on – while Rector et al. (2003a) have suggested larger viewing angles for HBLs based on smaller pc-to-kpc jet misalignments, Landt, Padovani & Giommi (2002) find no differences in viewing angles based on the Ca H&K break, an orientation indicator.

The lower apparent speeds observed in HBLs on their own could be taken to support the different angle scenario, since lower observed apparent speeds could come about if the HBL jets were viewed at larger angles to the line of sight (even if the intrinsic speeds of the HBLs and LBLs were basically the same). However, we find that the other differences that we observe between LBLs and HBLs cannot be reconciled with this simple picture. This suggests that HBL jets are intrinsically slower than LBLs. In this case, the HBL jets would have lower Doppler factors, and so, on average, would be viewed at a larger range of angles than the more Doppler-beamed LBL jets (but with this range being smaller than that for FR I radio galaxies). Thus, it is possible that the main effect leading to the differences in the apparent speeds is a systematic difference in intrinsic flow speed, but with the less important associated factor that the LBL jets are, on average, oriented at systematically smaller angles to line of sight, due to their increased beaming and subsequent prevalence in a flux-limited radio sample.

Note that Piner & Edwards (2004) have suggested that the high-energy TeV emission from the TeV blazars (mostly HBLs), which requires high Lorentz factors, can only be reconciled with the slow jet speeds inferred from radio observations if their jets are decelerating fast on microarcsecond scales, close to the central engine. This again supports the picture of intrinsically slower radio jets in HBLs compared to LBLs.

Several of our HBLs show evidence for 'spine-sheath' B field structures, with transverse B field in the inner region of the jet and longitudinal B field at the edges. Such structures have sometimes been interpreted as reflecting the velocity structure in a jet with a faster 'spine' and slower 'sheath' (e.g. Attridge et al. 1999). In this scenario, the more prominent longitudinal jet B fields in HBLs could come about if their jets are oriented at relatively larger angles to the line of sight, where the emission from the slower moving sheath field dominates, thus in principle supporting the 'different-angle scenario' for HBLs and LBLs. However, based on differences in the global properties of LBLs and HBLs, it seems much more likely that, if the longitudinal B field at the jet edges is due to shear, this comes about for some other reason, such as lower intrinsic speeds in HBL jets. In addition, as we consider below, such 'spine-sheath' B field structures may have an entirely different origin, having to do with the intrinsic B field of the jet.

7.2.2 Spine-shear jet structure and helical magnetic fields

Gabuzda et al. (2004) and Lyutikov et al. (2005) have pointed out that 'spine-sheath' structures of the sort observed for 1227+255 and 1727+502 could be observed if helical B fields are associated with the jets of these objects. In this case, the dominant observed B field orientation (aligned with or perpendicular to the jet) would be determined by the pitch angle of the helical B field, and also to some extent by the viewing angle. The pitch angle of the helical field might plausibly be determined, for example, by the relationship between the speed of rotation of the central black hole–accretion disc system and the outflow speed of the jets. One way to understand the differences in the observed jet B field structures of HBLs and LBLs is to suppose that this ratio tends to be lower for HBLs than for LBLs, resulting in smaller pitch angles for their jet B fields. This could come about, for example, if the rotational speed were *lower* and the outflow speed *higher* in HBLs than in LBLs.

The simplest interpretation of our tentative finding that HBLs seem to have lower superluminal speeds than LBLs is that the HBL jets have lower bulk Lorentz factors than the LBL jets. If true, their lower outflow speeds would tend to *increase* the pitch angles of the associated helical B fields (i.e. make their helical fields more tightly wound), which would lead to a tendency for their jet fields to be more, rather than less, dominated by a transverse field component. However, if the central rotational speeds of the HBLs are also lower than those in LBLs, the average ratio of the rotational to the outflow speeds could end up being lower in HBLs than in LBLs, tending to give rise to a dominant longitudinal field component.

In this picture, the characteristic jet Lorentz factors of HBLs would be systematically lower than those of LBLs and FSRQs. It is interesting that the VLBI jets of FSRQs also tend to show a predominance of longitudinal B fields. One way both the low-Lorentz-factor

HBLs and the high-Lorentz-factor FSRQs could end up with predominantly longitudinal jet *B* fields is if, in both cases, the ratio of the outflow to the central rotational speed is relatively high – in the HBLs due to relatively low rotational speeds, and in the quasars due to relatively high outflow speeds.

Indeed, the observed superluminal motions in quasar jets are, on average, somewhat higher than those in LBL jets (Gabuzda et al. 2000; Kellermann et al. 2004); the simplest interpretation of this systematic difference is that the typical jet Lorentz factors are higher in quasars than LBLs. Lower apparent speeds in LBLs could also come about if their jets were viewed at somewhat larger (or smaller) angles to the line of sight, but the former possibility is at odds with the high polarization and variability of LBLs, and the latter possibility would imply that LBLs should have higher Doppler factors than quasars, which is not the case. If HBLs display lower superluminal speeds than LBLs, and this reflects lower typical jet Lorentz factors in HBLs compared to LBLs, we find that FSRQs, LBLs and HBLs form a sequence of decreasing average jet Lorentz factor. Note that the order in this sequence is the same as that for the sequence in emission-line luminosity, from highest in FSRQs to lowest in HBLs (Ghisellini 1997), and also for the sequence of the synchrotron peak frequencies, from lowest for FSRQs to highest for HBLs.

If a jet does have a helical *B* field, this should give rise to a systematic gradient in the observed Faraday rotation measure across the jet, due to the systematic change in the line-of-sight *B* field component (Blandford 1993), as has been observed for several LBLs (Gabuzda et al. 2004). Multifrequency polarization VLBA data for the *HEAO-1* + RGB BL Lac objects considered here are currently being reduced; the detection of systematic rotation measure gradients transverse to the VLBI jets of any of these sources would appreciably strengthen the case that they are associated with helical *B* fields.

Meier et al. (1997) and Meier (1999) have demonstrated through numerical simulations that there may be a connection between the output radio power and the spin rate of the central black hole. Although the original idea was to explain the FR I and FR II classes, a similar idea could apply for the BL Lac subclasses. Objects with lower radio powers (i.e. the HBLs) could have black holes spinning at lower rates, which produce slower jets, while objects with higher radio powers (i.e. the LBLs) could have black holes spinning at higher rates, which produce relatively faster jets. In this picture, the unresolved bases of the jets, i.e. the radio 'cores', should be weaker in the HBLs, in agreement with our observations, while the radio cores of LBLs should be more dominant. We have already discussed above how differences in the black hole spin rates of HBLs and LBLs could lead to the observed differences in VLBP structure, if the jets have helical magnetic fields. In addition, there is the secondary effect that the less Doppler-beamed HBL jets would be oriented, on average, at somewhat larger angles to the line of sight than the more beamed LBLs (but always within a smaller range than for their unbeamed counterparts, the FR I radio galaxies). Thus, through all the observational manifestations and consequences that could plausibly follow from a difference in characteristic black hole spin rates, this one most fundamental difference may essentially be able to explain the observed properties of LBLs and HBLs. We will be exploring this scenario as a means of understanding the *B* field geometries observed in quasar subclasses as well (Lister 2001) in a future paper.

7.2.3 Misclassified quasars in the BL Lac populations

Some HBLs and LBLs have been found to have FR II radio powers and morphologies (Kollgaard et al. 1992; Murphy, Browne & Perley 1993), and it is possible that some subset of the HBLs and LBLs are actually misclassified radio quasars. However, there is no tendency for the HBLs that have longitudinal jet *B* fields also to have the lowest core polarizations, arguing against the idea that a large fraction of the HBLs are misclassified quasars. In addition, the observed superluminal speeds in quasars are clearly higher than the tentative speeds available for HBLs thus far.

7.2.4 Comparisons of BL Lac subclasses with similar B field structures

Gabuzda et al. (2000) have demonstrated that the pc-scale jet EVPAs in LBLs show a bimodal distribution – while the majority of LBLs exhibit transverse jet *B* fields, there is a subset of LBLs that exhibit a longitudinal *B* field morphology (see Fig. 20). We compared the properties of the HBLs with the subset of LBLs that show longitudinal *B* fields similar to the HBLs. We found that like the majority of LBLs, this subset of LBLs still show all the differences in their basic properties which are observed in the two subclasses as a whole, i.e. the LBL subset still have systematically higher redshifts, higher core fractional polarizations, greater component speeds, and no difference in the distribution of the jet fractional polarizations or core EVPAs compared to HBLs. This strongly supports the picture of intrinsic differences in the LBL and HBL classes.

8 CONCLUSIONS

(1) We have observed eighteen BL Lacs belonging to the *HEAO-1* and RGB samples with VLBI, and detected pc-scale polarization in all but three of them. After dividing each of our objects into the HBL or LBL classes and considering the known results on LBLs in the literature, we have carried out a comparison of the relevant properties of the two BL Lac classes.

(2) We find that the total intensity pc-scale images reveal a core–jet morphology, similar to that observed in LBLs.

(3) The VLBP observations of HBLs and LBLs reveal differences in their core fractional polarization, similar to the trend observed on kpc scales – the HBLs have a lower core fractional polarization compared to the LBLs. High degrees of core polarization were observed for the two RGB sources 0749+540 ($\simeq$10 per cent) and 0925+504 ($\simeq$14 per cent), but both of these are, in fact, LBLs.

(4) The jet fractional polarizations in HBLs do not differ systematically from those in LBLs. In both cases, jet degrees of polarization of tens of per cent can sometimes be observed, indicating the presence of well-ordered *B* fields.

(5) The relative VLBI core polarization angles do not show any systematic differences between HBLs and LBLs.

(6) The most intriguing difference between the HBLs and the LBLs is the orientation of the predominant *B* fields in their pc-scale jets – the *B* fields in HBL jets tend to be aligned with the local jet direction, while the *B* fields of LBLs tend to be perpendicular to the local jet direction. This result needs to re-examine with a larger sample of HBLs.

(7) Some of the HBLs display evidence for jet magnetic field structures with transverse *B* field in the inner region of the jet and longitudinal *B* field at the edges, i.e. a 'spine-sheath' structure. Although such *B*-field structures have been taken to indicate a fast spine + slow sheath velocity structure, they can also come about in a natural, simpler way if the jet has a helical *B* field (without any requirement for a two-layer velocity structure).

(8) We find tentative evidence that the observed component speeds in HBLs are lower than the typical apparent speeds observed

in LBLs ($\simeq 1c$–$5c$) and FSRQs ($\simeq 5c$–$10c$). This result suggests that either the HBL jets have lower Lorentz factors than LBLs and FSRQs, or that their jets are oriented at larger angles to the line of sight. Since the collected properties of HBLs provide no clear evidence that their jets lie at systematically larger angles to the line of sight than do LBL jets, this suggests that the outflow speeds are intrinsically lower in HBLs, than in LBLs.

(9) One way to understand our collected results in the context of other previous results in the literature is if HBLs, LBLs and FSRQs form a sequence of increasing average jet Lorentz factor – the same order as for the sequence of the synchrotron peaks of these objects, which proceed from highest peak frequency for HBLs to lowest peak frequency for FSRQs, although the physical connection between these two sequences is not clear.

(10) If the jets of all three classes of compact AGN characteristically have helical B fields due to the 'winding up' of a seed field via the combination of outflow and rotation of the central black hole–accretion disc system, then the dominant jet B fields observed in these three classes of compact AGN – longitudinal in HBLs and FSRQs and transverse in LBLs – could come about due to the ratios of their characteristic rotational and outflow velocities. If HBLs, LBLs and FSRQs do form a sequence of increasing Lorentz factor, the low outflow speeds in HBLs would require relatively slow rotation (i.e. smaller spin rates) of their central black hole–accretion disc systems.

ACKNOWLEDGMENTS

We would like to thank the referee, Eric Perlman, for a careful assessment of our work, which has greatly improved the paper. PK is grateful to the Joint Institute for VLBI in Europe (JIVE) for providing her with a summer studentship in 2001. We would like to acknowledge Ron Kollgaard's contribution in initiating the VLBP project. This research has made use of the NED which is operated by the Jet Propulsion Laboratory, California Institute of Technology, under contract with the National Aeronautics and Space Administration.

REFERENCES

Albert J. et al. (MAGIC Collaboration), 2007, ApJ, 667, L21
Antonucci R. R. J., Ulvestad J. S., 1985, ApJ, 294, 158
Attridge J. M., Roberts D. H., Wardle J. F. C., 1999, ApJ, 518, L87
Bade N., Beckmann V., Douglas N. G., Barthel P. D., Engels D., Cordis L., Nass P., Voges W., 1998, A&A, 334, 459
Blandford R. D., 1993, in Burgarella D., Livio M., O'Dea C. P., eds, Astrophysical Jets. Cambridge Univ. Press, Cambridge
Blandford R. D., Königl A., 1979, ApJ, 232, 34
Blandford R. D., Rees M. J., 1978, in Pittsburgh Conference on BL Lac Objects, Pittsburgh, PA, April 24–26, 1978, Proceedings. (A79-30026 11-90) Pittsburgh, PA, University of Pittsburgh, 1978, p. 328; Discussion, p. 341. NATO-supported research
Browne I. W. A., 1983, MNRAS, 204, 23P
Burbidge G., Hewitt A., 1987, AJ, 93, 1
Cawthorne T. V., Wardle J. F. C., Roberts D. H., Gabuzda D. C., 1993, ApJ, 416, 519
Charlot P., Gabuzda D. C., Sol H., Degrange B., Piron F., 2006, A&A, 457, 455
Costamante L., Ghisellini G., 2002, A&A, 384, 56
Donato D., Sambruna R. M., Gliozzi M., 2005, A&A, 433, 1163
Dondi L., Ghisellini G., 1995, MNRAS, 273, 583
Edwards P. G., Piner B. G., 2002, ApJ, 579, L67
Falomo R., 1991, AJ, 102, 1991
Falomo R., Tanzi E. G., 1991, AJ, 102, 1294
Falomo R., Scarpa R., Bersanelli M., 1994, ApJS, 93, 125
Fanaroff B. L., Riley J. M., 1974, MNRAS, 167, 31P
Fossati G., Maraschi L., Celotti A., Comastri A., Ghisellini G., 1998, MNRAS, 299, 433
Gabuzda D. C., 2003, Ap&SS, 288, 39
Gabuzda D. C., Wardle J. F. C., Roberts D. H., 1989, ApJ, 338, 743
Gabuzda D. C., Cawthorne T. V., Roberts D. H., Wardle J. F. C., 1992, ApJ, 388, 40
Gabuzda D. C., Mullan C. M., Cawthorne T. V., Wardle J. F. C., Roberts D. H., 1994, ApJ, 435, 140
Gabuzda D. C., Pushkarev A. B., Cawthorne T. V., 1999, MNRAS, 307, 725
Gabuzda D. C., Pushkarev A. B., Cawthorne T. V., 2000, MNRAS, 319, 1109
Gabuzda D. C., Murray É., Cronin P., 2004, MNRAS, 351, L89
Georganopoulos M., Marscher A. P., 1998, ApJ, 506, 621
George I. M., Warwick R. S., Bromage G. E., 1988, MNRAS, 232, 793
Ghisellini G., 1997, in Ostrowski M., Sikora M., Madejski G., Begelman M., eds, Relativistic Jets in AGNs Unification of All Blazars. Springer, Netherlands, p. 262
Ghisellini G., Maraschi L., 1989, ApJ, 340, 181
Ghisellini G., Tavecchio F., Chiaberge M., 2005, A&A, 432, 401
Giommi P., Padovani P., 1994, MNRAS, 268, L51
Giommi P. et al., 1989, in Maraschi L., Maccacaro T., Ulrich M.-H., eds, BL Lac Objects. Springer-Verlag, Berlin, p. 231
Giommi P., Piranomonte S., Perri M., Padovani P., 2005, A&A, 434, 385
Giroletti M. et al., 2004a, ApJ, 600, 127
Giroletti M., Giovannini G., Taylor G. B., Falomo R., 2004b, ApJ, 613, 752
Gregory P. C., Scott W. K., Douglas K., Condon J. J., 1996, ApJS, 103, 427
Heidt J., Nilsson K., Fried J. W., Takalo L. O., Sillanpää A., 1999, A&A, 348, 113
Henstock D. R., Browne I. W. A., Wilkinson P. N., McMahon R. G., 1997, MNRAS, 290, 380
Hewitt A., Burbidge G., 1987, ApJS, 63, 1
Hutter D. J., Mufson S. L., 1980, BAAS, 12, 486
Jannuzi B. T., Smith P. S., Elston R., 1994, ApJ, 428, 130
Jorstad S. G., Marscher A. P., Mattox J. R., Aller M. F., Aller H. D., Wehrle A. E., Bloom S. D., 2001, ApJ, 556, 738
Kapahi V. K., 1979, A&A, 74, L11
Kellermann K. I. et al., 2004, ApJ, 609, 539
Kock A., Meisenheimer K., Brinkmann W., Neumann M., Siebert J., 1996, A&A, 307, 745
Kollgaard R. I., Wardle J. F. C., Roberts D. H., Gabuzda D. C., 1992, AJ, 104, 1687
Kollgaard R. I., Gabuzda D. C., Feigelson E. D., 1996a, ApJ, 460, 174
Kollgaard R. I., Palma C., Laurent-Muehleisen S. A., Feigelson E. D., 1996b, ApJ, 465, 115
Kühr H., Schmidt G. D., 1990, AJ, 99, 1
Landt H., Padovani P., Giommi P., 2002, MNRAS, 336, 945
Laurent-Muehleisen S. A., Kollgaard R. I., Moellenbrock G. A., Feigelson E. D., 1993, AJ, 106, 875
Laurent-Muehleisen S. A., Kollgaard R. I., Ryan P. J., Feigelson E. D., Brinkmann W., Siebert J., 1997, A&AS, 122, 235
Laurent-Muehleisen S. A., Kollgaard R. I., Ciardullo R., Feigelson E. D., Brinkmann W., Siebert J., 1998, ApJS, 118, 127
Laurent-Muehleisen S. A., Kollgaard R. I., Feigelson E. D., Brinkmann W., Siebert J., 1999, ApJ, 525, 127
Ledden J. E., Odell S. L., 1985, ApJ, 298, 630
Liller M. H., Liller W., 1975, ApJ, 199, L133
Lister M. L., 2001, ApJ, 562, 208
Lister M. L., Homan D. C., 2005, AJ, 130, 1389
Lyutikov M., Pariev V. I., Gabuzda D. C., 2005, MNRAS, 360, 869
Maraschi L., Tavecchio F., 2001, in ASP Conf. Ser. Vol. 227, Blazar Demographics and Physics Spectral Energy Distributions of Blazars: Facts and Speculations. Astron. Soc. Pac., San Francisco, p. 40
Meier D. L., 1999, ApJ, 522, 753
Meier D. L., Edgington S., Godon P., Payne D. G., Lind K. R., 1997, Nat, 388, 350

Morris S. L., Stocke J. T., Gioia I. M., Schild R. E., Wolter A., Maccacaro T., della Ceca R., 1991, ApJ, 380, 49
Murphy D. W., Browne I. W. A., Perley R. A., 1993, MNRAS, 264, 298
Mushotzky R. F., Boldt E. A., Holt S. S., Serlemitsos P. J., Swank J. H., Rothschild R. H., Pravdo S. H., 1978, ApJ, 226, L65
Nass P., Bade N., Kollgaard R. I., Laurent-Muehleisen S. A., Reimers D., Voges W., 1996, A&A, 309, 419
Nieppola E., Tornikoski M., Valtaoja E., 2006, A&A, 445, 441
Nilsson K., Takalo L. O., Pursimo T., Sillanpää A., Heidt J., Wagner S. J., Laurent-Muehleisen S. A., Brinkmann W., 1999, A&A, 343, 81
Oke J. B., 1978, ApJ, 219, L97
Padovani P., Giommi P., 1995, MNRAS, 277, 1477
Padovani P., Urry C. M., 1990, ApJ, 356, 75
Padovani P., Costamante L., Ghisellini G., Giommi P., Perlman E., 2002, ApJ, 581, 895
Patnaik A. R., Browne I. W. A., Wilkinson P. N., Wrobel J. M., 1992, MNRAS, 254, 655
Perlman E. S., 1994, PhD thesis, Univ. Colorado, Boulder
Perlman E. S., Stocke J. T., 1993, ApJ, 406, 430
Perlman E. S., Stocke J. T., Wang Q. D., Morris S. L., 1996, ApJ, 456, 451
Perlman E. S., Padovani P., Giommi P., Sambruna R., Jones L. R., Tzioumis A., Reynolds J., 1998, AJ, 115, 1253
Pica A. J., Smith A. G., Webb J. R., Leacock R. J., Clements S., Gombola P. P., 1988, AJ, 96, 1215
Piner B. G., Edwards P. G., 2004, ApJ, 600, 115
Piner B. G., Edwards P. G., 2005, ApJ, 622, 168
Prestage R. M., Peacock J. A., 1988, MNRAS, 230, 131
Pushkarev A. B., 2001, Astron. Rep., 45, 667
Rector T. A., Stocke J. T., Perlman E. S., Morris S. L., Gioia I. M., 2000, AJ, 120, 1626
Rector T. A., Gabuzda D. C., Stocke J. T., 2003a, AJ, 125, 1060
Rector T. A., Gabuzda D. C., Stocke J. T., 2003b, AJ, 125, 1060
Reid R. I., Kronberg P. P., Perley R. A., 1999, ApJS, 124, 285
Reynolds C., Cawthorne T. V., Gabuzda D. C., 2001, MNRAS, 327, 1071
Roberts D. H., Gabuzda D. C., Wardle J. F. C., 1987, ApJ, 323, 536
Sambruna R. M., 1997, ApJ, 487, 536
Sambruna R. M., Maraschi L., Urry C. M., 1996, ApJ, 463, 444
Schwartz D. A., Griffiths R. E., Schwarz J., Doxsey R. E., Johnston M. D., 1979, ApJ, 229, L53
Schwartz D. A., Brissenden R. J. V., Tuohy T. R., Feigelson E. D., Hertz P. L., Remillard R. A., 1989, in Maraschi L., Maccacaro T., Ulrich M.-H., eds, BL Lac Objects. Springer-Verlag, Berlin, p. 209
Stein W. A., Odell S. L., Strittmatter P. A., 1976, ARA&A, 14, 173
Stevens J. A., Gear W. K., 1999, MNRAS, 307, 403
Stickel M., Kühr H., 1993, A&AS, 101, 521
Stickel M., Fried J. W., Kühr H., 1993, A&AS, 98, 393
Stocke J. T., Liebert J., Schmidt G., Gioia I. M., Maccacaro T., Schild R. E., Maccagni D., Arp H. C., 1985, ApJ, 298, 619
Stocke J. T., Morris S. L., Gioia I. M., Maccacaro T., Schild R. E., Wolter A., 1989, in Maraschi L., Maccacaro T., Ulrich M.-H., eds, BL Lac Objects. Springer-Verlag, Berlin, p. 242
Strittmatter P. A., Serkowski K., Carswell R., Stein W. A., Merrill K. M., Burbidge E. M., 1972, ApJ, 175, L7
Taylor G. B., Vermeulen R. C., Pearson T. J., Readhead A. C. S., Henstock D. R., Browne I. W. A., Wilkinson P. N., 1994, ApJS, 95, 345
Ulrich M.-H., 1978, ApJ, 222, L3
Ulrich M.-H., Kinman T. D., Lynds C. R., Rieke G. H., Ekers R. D., 1975, ApJ, 198, 261
Ulvestad J. S., Johnston K. J., 1984, AJ, 89, 189
Ulvestad J. S., Johnston K. J., Weiler K. W., 1983, ApJ, 266, 18
Urry C. M., Padovani P., 1995, PASP, 107, 803
Urry C. M., Padovani P., Stickel M., 1991a, ApJ, 382, 501
Urry C. M., Padovani P., Stickel M., 1991b, ApJ, 382, 501
van Gorkom J. H., Knapp G. R., Ekers R. D., Ekers D. D., Laing R. A., Polk K. S., 1989, AJ, 97, 708
Veron-Cetty M.-P., Veron P., 1993, ESO Scientific Report, A Catalogue of Quasars and Active Nuclei, 6th edn. European Southern Observatory (ESO), Garching, }c1993
Wardle J. F. C., Moore R. L., Angel J. R. P., 1984a, ApJ, 279, 93
Wardle J. F. C., Moore R. L., Angel J. R. P., 1984b, ApJ, 279, 93
Wood K. S. et al., 1984, ApJS, 56, 507
Wu Z., Jiang D. R., Gu M., Liu Y., 2007, A&A, 466, 63
Wurtz R., Stocke J. T., Yee H. K. C., 1996, ApJS, 103, 109
Zavala R. T., Taylor G. B., 2003, ApJ, 589, 126
Zavala R. T., Taylor G. B., 2004, ApJ, 612, 749

This paper has been typeset from a TEX/LATEX file prepared by the author.